Activated rate processes: The reactive flux method for one-dimensional surface diffusion

Joel S. Bader and B. J. Berne
Department of Chemistry, Columbia University, New York, New York 10027

Eli Pollak
Chemical Physics Department, The Weizmann Institute of Science, 76100 Rehovot, Israel

(Received 22 February 1994; accepted 1 December 1994)

We have implemented a semiclassical dynamics simulation method to investigate the effects of finite barrier heights and nonlinear potentials on the rate of diffusion of a particle which is coupled to a frictional bath and is traveling on a one-dimensional potential energy surface. The classical reactive flux method has been modified to account for semiclassical tunneling and above-barrier reflection. A novel perturbation theory treatment of the semiclassical dynamics is developed to simulate the motion of the particle when the coupling to the frictional bath is small and the particle's motion is nearly conservative. Our simulation results support the theoretical prediction that the diffusion constant increases as friction decreases. We also find supporting evidence for an inverse isotope effect, as the diffusion constant for a classical particle can be larger than that of a corresponding quantum mechanical particle. The escape rate and the average energy of escaping particles are also found to be in good agreement with theoretical predictions.

I. INTRODUCTION

The theory of surface diffusion has been extensively developed during recent years.[1,2] The reactive flux formalism for activated rate processes,[3–12] deeper insight into transition state theory, efficient numerical methods,[13–15] and detailed numerical simulations have considerably increased understanding of the role of surface potential, phonon interactions and surface structure on diffusion. The diffusion process is often considered as a random walk, limited by the rate it takes the atom or molecule to hop from one site to an adjacent one on the surface. The diffusion coefficient is proportional to this activated escape rate. Theoretical effort was primarily aimed at accurate estimates for the rate. When the particle is a chemically bound species with a relatively high barrier separating adjacent sites, this may be a daunting task.

A different but important aspect is the fate of the particle once it has escaped from a well. The particle may execute multiple hops before retrapping in a different well.[10] Such multiple hops will significantly enhance the diffusion coefficient. In most simulation studies though, such correlated hops were rarely found. Recent experimental[16] and numerical[17] studies have indicated that correlated hops should not be neglected and could strongly influence the diffusion coefficient. The experimental work of Ganz *et al.*[16] using scanning tunneling microscopy (STM) methods seems to demonstrate correlated hopping of Pb on a reconstructed Ge(111) surface. In their numerical study of the diffusion of CO on a Ni(111) surface, Dobbs and Doren[17] have found that correlated hops significantly affect the diffusion coefficient. Correlated hops over ten adjacent sites were observed.

One-dimensional surface diffusion has been studied recently by Ferrando *et al.*[18,19] In their model, the motion of a particle on a one-dimensional infinite periodic lattice is governed by a Langevin equation. The interaction of the particle with the surface phonon modes is modeled as a random force which is related to the friction by the fluctuation-dissipation relation. In the weak damping limit, they find that correlated hops are dominant, and lead to a divergence of the classical diffusion coefficient. Moro and Polimeno[20] recently investigated correlated hopping in the presence of a periodic potential with four wells. They were modeling the *trans-gauche* isomerization of *n*-butane and found that the ratio of two-barrier to one-barrier crossings increases significantly as the damping becomes weaker.

Correlated hops in the underdamped limit are caused by the activation process. As shown by Büttiker, Harris, and Landauer,[21] the average classical energy of an escaping particle is proportional to the square root of the damping. As the particle traverses from one barrier to the next along the periodic potential its energy loss is linearly proportional to the damping. The consequence is that the escaping particle will cross many barriers before losing enough energy to be again retrapped.

We have recently shown[22] that the classical correlated hopping probability is of the order of unity in the classical underdamped limit. This finding was consistent with the experimental observations of Ganz *et al.* who measured a correlated hopping probability of at least 0.5. We also found that the quantum correlated hopping probability is smaller than the classical. Quantum tunneling causes a lowering of the average energy of the escaping particle thus decreasing the contribution of correlated hopping.

Mel'nikov[23,24] has studied the classical motion of a particle on a tilted potential. His results were recently extended[25] to provide a semiclassical theory of surface diffusion above the crossover temperature[11,26,27] between quantum tunneling and thermal activation. Explicit expressions for the rate of escape (Γ), the partial rate Γ_j for being retrapped after moving a distance jl_0 (l_0 is the distance between adjacent wells), the mean squared path length $\langle l^2 \rangle$ and the diffusion coefficient D were provided. In the underdamped limit, above-barrier reflection and below-barrier tun-

 0021-9606/95/102(10)/4037/19/$6.00 © 1995 American Institute of Physics

neling cause the quantum correlated hopping probability to be lower than the classical probability, and the quantum diffusion constant is lower than the classical prediction.

We have attempted to verify and extend these theoretical developments using direct numerical integration of the Langevin equation and found that especially in the underdamped limit, it is rather difficult to obtain accurate statistics. We were also interested in providing a numerical technique which would include the quantum effects. The central purpose of the present paper is to extend the reactive flux method to directly address these difficulties. In contrast to the analytic studies, the methods we describe have the advantage of being readily amenable to the study of surface diffusion in more than one dimension. We will use the numerical method to verify and extend the analytic theory presented in Refs. 22, 25.

A secondary purpose of this paper is to present the theory described only briefly in Ref. 22. The analytic theory is reviewed in Section II. The mathematical methods used in Section II to extract analytical expressions for escape rates and correlated hopping probabilities are not essential for a physical understanding of the results we obtain. Readers not interested in the details of the analytical techniques might wish to skip this section, noting only the analytical expressions we obtain for the escape rate and the diffusion constant. An extension of the reactive flux method which incorporates semiclassical transmission and reflection is presented in Section III, along with an efficient new algorithm for propagating trajectories when friction is small. Section IV serves to define the observables we compute, and in Section V the simulation results are reported. We end with a summary and a discussion of future directions and extensions.

II. CORRELATED HOPPING AND SURFACE DIFFUSION

A. The escape rate

The model to be considered is that of a particle with mass m trapped in the well of the potential $w(q)$ (q is the particle coordinate). A Generalized Langevin Equation (GLE) governs the dynamics,

$$\ddot{q}+\frac{1}{m}\frac{dw(q)}{dq}+\int^{t} d\tau\gamma(t-\tau)\dot{q}(\tau)=\frac{1}{m}\,\xi(t). \tag{2.1}$$

The Gaussian random force $\xi(t)$ with zero mean is related to the time dependent friction function $\gamma(t)$ through the fluctuation dissipation relation:

$$\langle\xi(t)\xi(t')\rangle=\frac{m}{\beta}\,\gamma(t-t') \tag{2.2}$$

and $\beta\equiv 1/k_BT$.

The quantum rate for hopping out of one of the wells at temperatures above the crossover temperature ($\hbar\lambda^{\ddagger}/k_BT\leqslant 2\pi$) is[28]

$$\Gamma=\frac{\omega_0}{\pi}\,e^{-\beta V^{\ddagger}}\frac{\lambda^{\ddagger}}{\omega^{\ddagger}}\,\Xi\Upsilon. \tag{2.3}$$

Here, $\lambda^{\ddagger}$ is the Kramers–Grote–Hynes reactive frequency,[29–31]

$$\frac{\lambda^{\ddagger}}{\omega^{\ddagger}}=\left[1+\frac{\hat{\gamma}(\lambda^{\ddagger})}{\lambda^{\ddagger}}\right]^{-1/2}, \tag{2.4}$$

where the hat denotes the Laplace transform of the time dependent friction. The ratio of quantum to classical partition functions[32] at the barrier and the well (Ξ) is expressed in terms of the Matsubara frequencies $\tilde{\omega}_n\equiv 2\pi n/\hbar\beta$ and the Laplace transform of the time dependent friction

$$\Xi\equiv\prod_{n=1}^{\infty}\frac{[\omega_0^2+\tilde{\omega}_n^2+\tilde{\omega}_n\hat{\gamma}(\tilde{\omega}_n)]}{[-\omega^{\ddagger 2}+\tilde{\omega}_n^2+\tilde{\omega}_n\hat{\gamma}(\tilde{\omega}_n)]}. \tag{2.5}$$

The "depopulation factor" Υ is

$$\Upsilon=\exp\left[a^{-1}\sin\left(\frac{\pi}{a}\right)\int_{-\infty}^{\infty}dt\,\frac{\ln\left[1-\tilde{P}\left(t-\frac{i}{2}\right)\right]}{\cosh\left(\frac{2t\pi}{a}\right)-\cos\left(\frac{\pi}{a}\right)}\right] \tag{2.6}$$

and the quantum parameter $a\equiv 2\pi/\hbar\beta\lambda^{\ddagger}$.

The magnitude of the depopulation factor is mainly determined by the probability kernel $P(E|E')$ which expresses the probability density that a particle with energy E' initially in the vicinity of a barrier will reach the next barrier with energy E. The two sided Laplace transform of this kernel which appears in the expression for the depopulation factor is defined as

$$\tilde{P}(is)\equiv\int_{-\infty}^{\infty}d\epsilon e^{-s(\epsilon-\epsilon')}P(\epsilon|\epsilon'). \tag{2.7}$$

In the classical limit the probability kernel (using the dimensionless energy variable $\epsilon\equiv\beta E$) is a Gaussian function,

$$P(\epsilon|\epsilon')=\left(\frac{1}{4\pi\delta}\right)^{1/2}\exp\left[-\frac{(\epsilon+\delta-\epsilon')^2}{4\delta}\right]. \tag{2.8}$$

The reduced average energy loss (δ) of the particle as it traverses from one barrier to the next depends on the damping and the particular form of the periodic potential. In the weak to moderate damping limit the energy loss is well approximated as[33]

$$\delta=\frac{\beta m}{2}\int_{-\infty}^{\infty}dt\int_{-\infty}^{\infty}dt'\,\gamma(t-t')\dot{q}(t)\dot{q}(t'). \tag{2.9}$$

The trajectory $q(t)$ is the trajectory for the particle coordinate at the barrier energy in the absence of coupling to the bath.

In the classical limit, the depopulation factor simplifies considerably:[34]

$$\Upsilon_{\rm cl}=\exp\left[\frac{1}{\pi}\int_0^{\infty}\frac{dx}{x^2+1/4}\ln(1-e^{-\delta(x^2+1/4)})\right]. \tag{2.10}$$

In the underdamped limit ($\delta\ll 1$), one finds that $\Upsilon_{\rm cl}\simeq\delta$. This reflects the large reduction of the escape rate due to the very slow energy diffusion process. The quantum depopulation factor is *larger* than its classical counterpart in the underdamped limit, $\Upsilon\simeq\delta^{1-\hbar\beta\lambda^{\ddagger}/2\pi}$.[28,35] In the spatial diffusion

limit ($\delta > 1$), the energy relaxation rate is fast and the classical and quantum depopulation factors are unity. This allows us to define the spatial diffusion rate Γ_{sd} as

$$\Gamma_{sd} \equiv \frac{\Gamma}{Y}. \tag{2.11}$$

The quantum rate is found by solving a master equation for the population per unit time of particles $f(\epsilon)$ with (reduced) energy ϵ at the top of the barrier.[28,33] For a periodic potential one must in principle write down a coupled set of master equations for populations at each barrier.[23,25] However, both in the underdamped limit as well as in the overdamped limit, backscattering from adjacent wells is negligible.[18,19] To obtain the rate, or the average energy of escaping particles, it is sufficient to consider the analogous single well case, ignoring any backscattering. The validity of this simplifying assumption will be discussed in further detail in Section IV. The result is that one can consider the usual integral equation[28]

$$f(\epsilon) = \int_{-\infty}^{\infty} d\epsilon' P(\epsilon|\epsilon') R(\epsilon') f(\epsilon'), \tag{2.12}$$

where $R(\epsilon)$ is the quantum reflection probability for a parabolic barrier:

$$R(\epsilon) = [1 + \exp(a\epsilon)]^{-1}. \tag{2.13}$$

The transmission coefficient $T(\epsilon) = 1 - R(\epsilon)$. The integral equation is subject to the boundary condition that deep in the well the distribution $f(\epsilon)$ is in thermal equilibrium. It is solved using two sided Laplace transforms. The solution for the distribution is[28]

$$\tilde{N}(is) = -\frac{(\pi C/a)}{\sin\left[\frac{\pi(s+1)}{a}\right]} \exp\left[\frac{1}{2ia}\int_{z-i\infty}^{z+i\infty} dy \, \ln[1-\tilde{P}(iy)] \times \left[\cot\left(\pi\,\frac{s-y}{a}\right) + \cot\left(\pi\,\frac{y+1}{a}\right)\right]\right], \tag{2.14}$$

where we have used the notation

$$N(\epsilon) \equiv 2\pi\hbar\beta R(\epsilon) f(\epsilon) \tag{2.15}$$

and the constant C is

$$C \equiv 2\frac{\omega_0}{\omega_b} \sin\left(\frac{\hbar\beta\lambda^{\ddagger}}{2}\right) \Xi e^{-\beta V^{\ddagger}}. \tag{2.16}$$

The restriction on the real limits of the integration is

$$z > \mathrm{Re}(s) > z - a, \quad z > -1. \tag{2.17}$$

The rate is given by summation over all particles transmitted per unit time:

$$\Gamma = \int_{-\infty}^{\infty} d\epsilon T(\epsilon) f(\epsilon), \tag{2.18}$$

and this leads to Eqs. (2.3)–(2.6) given above as shown in Appendix A of Ref. 28.

One of the important new results presented in Ref. 22 is an expression for the quantum average energy of particles crossing the barrier. Here we provide a more detailed derivation. The average energy is defined as

$$\langle \epsilon \rangle \equiv \frac{\int_{-\infty}^{\infty} d\epsilon \epsilon T(\epsilon) f(\epsilon)}{\int_{-\infty}^{\infty} d\epsilon T(\epsilon) f(\epsilon)}. \tag{2.19}$$

Using the fact that

$$2\pi\hbar\beta T(\epsilon) f(\epsilon) = e^{a\epsilon} N(\epsilon) \tag{2.20}$$

and resorting to the two sided Laplace transform one finds that the average energy of transmitted particles may be obtained by the relation

$$2\pi\hbar\beta\Gamma\langle\epsilon\rangle = -\frac{d}{ds}\,\tilde{N}(is)|_{s=-a}. \tag{2.21}$$

Inserting the expression for $\tilde{N}$ (cf Eq. 2.14) one finds the explicit result

$$\langle \epsilon \rangle = \frac{\pi}{a}\left(\cot\left(\frac{\pi}{a}\right) + \frac{1}{a}\int_{-\infty}^{\infty} dx \, \ln\left[1 - \tilde{P}\left(x - \frac{i}{2}\right)\right] \times \frac{1 - \cosh\left(\frac{2\pi x}{a}\right)\cos\left(\frac{\pi}{a}\right)}{\left[\cosh\left(\frac{2\pi x}{a}\right) - \cos\left(\frac{\pi}{a}\right)\right]^2}\right) \tag{2.22}$$

which is the quantum generalization of the classical expression for the average energy derived by Mel'nikov and Meshkov.[34]

In the classical limit, Mel'nikov and Meshkov[34] demonstrated that $\langle\epsilon\rangle \simeq \delta^{1/2}$ in qualitative agreement with the prediction of Büttiker, Harris and Landauer.[21] In the quantum case, the average energy in the underdamped limit as elucidated from Eq. (2.22) is smaller, $\simeq \ln \delta$, and is negative with respect to the barrier height ($\epsilon = 0$), indicating that the quantum particles in the underdamped limit tend to escape by tunneling.

B. The correlated hopping probability

When a particle escapes from the well across a barrier (denoted as 1) it will continue towards the adjacent well and barrier (denoted as 2). It will then either get immediately trapped in the well (the typical case in the strong damping limit), it might be reflected by barrier 2, or it might continue directly across barrier 2. The correlated hopping probability P_1 is *defined* as the probability that the particle will continue across barrier 2 without being first trapped or reflected by the barrier:

$$P_1 = \frac{\int_{-\infty}^{\infty} d\epsilon \int_{-\infty}^{\infty} d\epsilon' T(\epsilon) P(\epsilon|\epsilon') T(\epsilon') f(\epsilon')}{\int_{-\infty}^{\infty} d\epsilon' T(\epsilon') f(\epsilon)}. \tag{2.23}$$

By using the Laplace transformed expressions and Eq. (2.20) one may rewrite the expression for the correlated hopping probability as

$$h\beta\Gamma P_1=\frac{1}{2\pi i}\int_{p-i\infty}^{p+i\infty} ds\tilde{P}(is)\tilde{R}[-i(a+s)]\tilde{N}[i(s-a)]. \tag{2.24}$$

The transform of the reflection coefficient is a standard integral:

$$\tilde{R}[-i(a+s)]=\frac{1}{a}\int_{-\infty}^{\infty} dx\ \frac{e^{(s/a)x}}{1+e^{-x}}=-\frac{\pi}{a}\frac{1}{\sin\left(\frac{s\pi}{a}\right)} \tag{2.25}$$

which converges provided that $\mathrm{Re}(s)<0$.

An explicit expression for the correlated hopping probability is derived by choosing $z=-1/2$ when inserting Eq. (2.14) in Eq. (2.24), introducing the change of variables

$$x\equiv i(y-z)\equiv i(y+\tfrac{1}{2}) \tag{2.26}$$

where x is pure real and

$$t\equiv i(s-p),\quad p=-\tfrac{1}{2}+A,\quad 0<A<\tfrac{1}{2}, \tag{2.27}$$

where t,A are also pure real. Taking the limit $A\to 0_+$, making use of the known identity

$$\lim_{A\to 0_+}\frac{t-x-iA}{(t-x)^2+A^2}=PP\left(\frac{1}{t-x}\right)-i\pi\delta(t-x), \tag{2.28}$$

and noting that the quantum kernel $\tilde{P}(t-i/2)$ is symmetric in the variable t gives the result

$$P_1=\frac{1}{2a}\sin\left(\frac{\pi}{a}\right)\frac{1}{\Upsilon^{1/2}}\int_{-\infty}^{\infty}dt\ \frac{\tilde{P}\left(t-\frac{i}{2}\right)\left[1-\tilde{P}\left(t-\frac{i}{2}\right)\right]^{1/2}}{\left[\sin^2\left(\frac{\pi}{2a}\right)+\sinh^2\left(\frac{\pi t}{a}\right)\right]}$$
$$\times\cos\left(\frac{1}{4\pi}\int_{-\infty}^{\infty}dw\ \frac{1}{w}\ \ln\left(\frac{1-\tilde{P}\left[(t-w)-\frac{i}{2}\right]}{1-\tilde{P}\left[(t+w)-\frac{i}{2}\right]}\right)\right.$$
$$\left.\times\left[\frac{\pi w}{a}\coth\left(\frac{\pi w}{a}\right)\right]\right). \tag{2.29}$$

The classical limit for the correlated hopping probability is readily seen to be

$$P_{1_{\mathrm{cl}}}=\Upsilon_{\mathrm{cl}}^{-1/2}\frac{1}{2\pi}\int_{-\infty}^{\infty}dt\ \frac{e^{-\delta(t^2+1/4)}[1-e^{-\delta(t^2+1/4)}]^{1/2}}{t^2+1/4}$$
$$\times\cos\left[\frac{1}{4\pi}\int_{-\infty}^{\infty}dw\ \frac{1}{w}\ \ln\left(\frac{1-e^{-\delta[(w-t)^2+1/4]}}{1-e^{-\delta[(w+t)^2+1/4]}}\right)\right]. \tag{2.30}$$

The classical correlated hopping probability is a function of a single parameter, the energy loss δ. In the high friction limit ($\delta\gg 1$) the classical correlated hopping probability becomes exponentially small:

$$P_{1_{\mathrm{cl}}}\simeq\frac{2}{(\delta\pi)^{1/2}}e^{-\delta/4}. \tag{2.31}$$

In the weak damping limit, the correlated hopping probability goes to a constant ($\simeq 0.7$). The quantum correlated hopping probability differs dramatically from the classical: it goes to zero in the underdamped limit.

The diffusion coefficient is well defined when the mean squared path length of a trajectory initiated in a well grows linearly with time and is by definition the proportionality constant. To compute the diffusion coefficient one assumes a separation of time scales. The longest time scale is the escape time $\tau_{\mathrm{rxn}}\equiv\Gamma^{-1}$. Once a particle has escaped from a well it will take an additional amount of time—τ_{trap}—before it is retrapped in any well. A particle that is trapped will again escape after a time which is of the order of τ_{rxn}. One assumes that $\tau_{\mathrm{trap}}\ll\tau_{\mathrm{rxn}}$. During the trapping time the particle will traverse a mean squared distance $\langle l^2\rangle$. The diffusion coefficient is

$$D=\tfrac{1}{2}\Gamma\langle l^2\rangle. \tag{2.32}$$

Within the time τ_{trap} before an activated particle is trapped, its trajectory may be composed of several segments in which the particle moves in a constant direction. The probability that such a segment is longer than one lattice spacing, for example, is what we have termed the correlated hopping probability P_1. The mean square jump length $\langle l^2\rangle$ is obtained from the distribution of jump lengths between escape and retrapping, not from the distribution of lengths of the correlated segments.

The result for the quantum diffusion coefficient is found to be[25]:

$$\frac{D}{D_{\mathrm{sd}}}=\Upsilon^{-1}\exp\left[a^{-1}\sin\left(\frac{\pi}{a}\right)\int_{-\infty}^{\infty}dt\right.$$
$$\left.\times\frac{\ln\left[1+\tilde{P}\left(t-\frac{i}{2}\right)\right]}{\cosh\left(\frac{2t\pi}{a}\right)-\cos\left(\frac{\pi}{a}\right)}\right]. \tag{2.33}$$

Here D_{sd} is the diffusion coefficient in the spatial diffusion limit:

$$D_{\mathrm{sd}}=\tfrac{1}{2}\Gamma_{\mathrm{sd}}l_0^2 \tag{2.34}$$

where l_0 is the distance between adjacent wells of the periodic potential. The mean squared path length may now be extracted from Eq. (2.32), since the diffusion coefficient and the rate are known.

C. Ohmic friction and a periodic potential

At this point, any practical computation necessitates knowledge of the quantum kernel whose details are determined by the specific potential and friction. A useful model is that of the symmetric cosine potential

$$w(q) = -\frac{V^{\ddagger}}{2}\left[1+\cos\left(\frac{2\pi q}{l_0}\right)\right], \tag{2.35}$$

for which the barrier frequency is identical to the well frequency:

$$\omega^{\ddagger 2} = \frac{2\pi^2}{m l_0^2}\, V^{\ddagger}. \tag{2.36}$$

For Ohmic friction,

$$\gamma(t) = 2\gamma\delta(t) \tag{2.37}$$

(where $\delta(t)$ is the Dirac "δ" function and should not be confused with the energy loss parameter δ), we show in the appendix that the quantum kernel has the form[28]

$$\tilde{P}\left(t-\frac{i}{2}\right) \equiv \exp[-r(t)], \tag{2.38}$$

where the exponent is obtained by a quadrature:

$$r(t) = \frac{\pi\delta}{4\hbar\beta\omega^{\ddagger}}\int_{-\infty}^{\infty}\frac{d\lambda}{\lambda}\,\frac{1}{\cosh^2\left(\frac{\pi\lambda}{2\omega^{\ddagger}}\right)} \times \frac{\cosh(\frac{1}{2}\hbar\beta\lambda)-\cos(t\hbar\beta\lambda)}{\sinh(\frac{1}{2}\hbar\beta\lambda)}. \tag{2.39}$$

The quantum depopulation factor and diffusion coefficient are obtained by a double integral, and the quantum correlated hopping probability is obtained by numerical integration of a triple integral.

III. SIMULATION METHODS

Here we describe the Langevin dynamics methods we have developed for simulating motion in a one-dimensional potential,

$$\ddot{q} + \gamma\dot{q} + (1/m)dV(q)/dq = R(t), \tag{3.1}$$

and for including semiclassical tunneling and reflection in the dynamics. The classical Langevin equation is equivalent to the GLE, Eq. (2.1), for Ohmic friction, $\gamma(t-t') = 2\gamma\delta(t-t')$. The Gaussian random force $R(t)$ for a classical bath has zero mean and second moment $\langle R(t)R(t')\rangle = (2\gamma/\beta m)\,\delta(t-t')$. In Section VI we discuss possible extensions of the simulation method to treat a quantum mechanical bath.

We have selected a Langevin dynamics algorithm particularly suited for reactive flux simulations and describe the algorithm in Section III A. We also describe how semiclassical barrier transmission is implemented for a one-dimensional reaction coordinate in terms of a transmission probability $T(E)$. When the frictional damping and the random force are small, the stochastic motion of a particle under Langevin dynamics is nearly identical to conservative motion in the potential $V(q)$. In Section III B, we describe how (for weak friction) the effects of the frictional bath can be incorporated as a perturbative correction to a conservative reference trajectory. This method, which we term energy space dynamics, is much more efficient than a straightforward integration of the stochastic equations of motion. The subject of Section III C is how the tunneling probability $T(E)$ is obtained. The reactive flux method for studying activated escape of a classical particle must be modified when nonclassical barrier transmission is allowed. We derive a reactive flux method for semiclassical dynamics in Section III D.

These techniques permit the use of simulations to probe corrections to quantum mechanical transition state theory due to low barrier heights and nonlinear potentials. We can also investigate diffusion at temperatures slightly below the crossover temperature, the temperature at which the rate expressions developed in Section II cease to converge.

A. Semiclassical Langevin dynamics algorithm

For integrating the stochastic Langevin equation we have used an algorithm which reduces to the velocity Verlet algorithm as the friction $\gamma \to 0$. This algorithm is given as Eqs. (9.24a) and (9.24b) in Ref. 36. There are many other Verlet-like algorithms (see Ref. 36). The velocity Verlet-like algorithm steps from the position and velocity at one time to the position and velocity at the next time, particularly suiting it for reactive flux simulations. Velocity and position displacements due to the random force are chosen from an appropriate bivariate Gaussian distribution.[37]

When performing a Langevin simulation, it is important that the errors introduced by the integration scheme are much smaller than the size of typical variations in the trajectory due to the stochastic force. One measure of the error of the integration is the variation of the energy of the particle, $E = m\dot{q}^2/2 + V(q)$, when there is no friction. We chose the time step of the simulation so that this variation was at least an order of magnitude smaller than the expected energy loss of the particle over one traversal of a well near the barrier energy. For the simulations we report, a time step of $\tau/200$ was sufficient to conserve energy to better than $10^{-2}k_BT$; τ here is the period of oscillation of a particle with about k_BT of energy.

To account for tunneling in direct Langevin simulations, the velocity $\dot{q}(t)$ is compared with the velocity $\dot{q}(t+\delta t)$ after a single time step δt. If the product is negative, if $\dot{q}(t)$ points in the direction of the closest barrier, if the energy of the particle at time $t+\delta t$ is smaller than the barrier energy, and if a random number uniform on $[0,1]$ is less than $T[E(t+\delta t)]$, then q is assumed to have tunneled to the next well in the direction $\dot{q}(t)$. It starts moving away from the turning point in the next well with energy $E(t+\delta t)$. To account for reflection, if $q(t)$ and $q(t+\delta t)$ are on opposite sides of a barrier top, and if a random number uniform on $[0,1]$ is greater than $T[E(t+\delta t)]$, then the particle is assumed to have been reflected. It is returned to the $q(t)$ side of the barrier and starts moving back with energy $E(t+\delta t)$.

B. Semiclassical simulations in energy space

As is evident from the discussion above, when the friction is small most of the computational effort in a Langevin dynamics simulation involves integrating the nearly conservative equations of motion. It is much more efficient to ob-

tain the exact dynamics of the bare system coordinate, and to incorporate the effects of the friction and random force as a perturbation.

A perturbation theory for the change in the energy of a particle over the period of an oscillation is presented in Appendix II. The method for simulations in energy space is as follows. A particle starts with energy E at q_a, which is a barrier top or a turning point. The action $J(E)$ to reach the next barrier top or turning point q_b is calculated for the conservative dynamics $\ddot{q}=-(1/m)dV/dq$. A new energy E' is chosen from the distribution

$$P(E'|E)=\frac{\exp[-(E'-E-\Delta)^2/2\sigma^2]\Theta(E'-E_0)}{\int_{E_0}^{\infty}dE'\ \exp[-(E'-E-\Delta)^2/2\sigma^2]} \tag{3.2}$$

with $\sigma^2=2\gamma k_B T J(E)$ and $\Delta=-\gamma[J(E)-J(k_BT)]$. The Heaviside function $\Theta(E')$ restricts E' to values larger than E_0, the energy at the bottom of the well.[38] This kernel is not microscopically reversible since the parameters Δ and σ^2 are not symmetric in their dependence on E and E'. Although the kernel violates detailed balance, the deviations are small when the energy loss itself is small. As we discuss in Appendix II, we have checked that the small deviations from detailed balance do not affect our simulation results.

Given the new energy E', a random number uniform on $[0,1]$ is compared to the transmission probability $T(E')$. If the random number is less than $T(E')$, the particle crosses the barrier into the next well; if it is less than $T(E')$, the particle is reflected back into the well. Finally, a time counter is incremented by the amount $t=\int_{q_a}^{q_b}dq(dt/dq)=dJ(E)/dE$. This is in essence an extreme form of a multiple time scale simulation[15,39,40] with an adaptive step size equal to the energy-dependent period of motion.

Further insight into this dynamics scheme can be gained by regarding it as providing the exact solution of the integral equation, Eq. (2.12), which gives the stationary-state flux hitting the barrier of a metastable well, or, for diffusion on a periodic surface, the integral equation for the flux in each of the wells.[25] Let (n,d,E) stand for the state of the dynamical system at the start of a step. The energy is E, the direction of travel d is ± 1, and the particle is moving into well n from the barrier between well n and well $n-d$. The state (n',d',E') at the start of the next time step is taken from the distribution

$$\{\delta_{n',n+d}\delta_{d',d}T(E')+\delta_{n',n}\delta_{d',-d}[1-T(E')]\}P(E'|E). \tag{3.3}$$

The first term is the transmission of the particle into the next well; the second term is reflection back into the initial well; and δ here is the Kronecker delta function.

C. Semiclassical barrier transmission

The quantum barrier crossing effects of transmission and reflection have been included in the semiclassical dynamics algorithms in Sections III A and III B through $T(E)$. This is the probability that a particle impinging on a barrier $V(q)$ with energy E will be transmitted through the barrier. According to the semiclassical JWKB approximation,[41,42]

$$T(E)=\{1+\exp[2K(E)/\hbar]\}^{-1}. \tag{3.4}$$

Assuming that the maximum of the barrier is at $q^{\ddagger}$ and that $V(q^{\ddagger})=V^{\ddagger}$, the action integral $K(E)$ is

$$K(E)=\begin{cases}\displaystyle\int_{q_l}^{q_r}dq\sqrt{2m[V(q)-E]}, & E\leqslant V^{\ddagger};\\ \displaystyle-\int_{q_l^{\bigstar}}^{q_r^{\bigstar}}dq\sqrt{2m[E-V(q_b+iq^{\bigstar})]}, & E>V^{\ddagger}.\end{cases} \tag{3.5}$$

For $E\leqslant V^{\ddagger}$, q_l and q_r are the left and right turning points at the barrier, $q_l<q^{\ddagger}<q_r$, and $V(q_l)=V(q_r)=E$. For $E>V^{\ddagger}$, the solutions to $V(q)=E$, $q^{\ddagger}+iq_l^{\bigstar}$ and $q^{\ddagger}+iq_r^{\bigstar}$, fall in the complex plane, with $\mathrm{Re}(q_l^{\bigstar})<0$ and $\mathrm{Re}(q_r^{\bigstar})>0$.

The JWKB formula for $T(E)$ must be modified when the coordinate q is coupled to a frictional bath. It has been shown that frictional damping decreases the amount of tunneling.[32,43–48] The same result can also be derived in terms of the local normal modes of the Hamiltonian near the barrier top.[49] For the underdamped regime we study, however, the frictional coupling is small and $T(E)$ for the unstable normal mode is not much different from $T(E)$ for the undamped bare reaction coordinate. We introduce a frictional correction to the undamped $T(E)$ which we expect to be accurate for weak to moderate friction.

In order to correct $T(E)$ for a general nonlinear barrier, we first obtain an effective harmonic frequency ω' for the barrier. The effective frequency for energy E is chosen to give the same action $K(E)$ as the nonlinear barrier,

$$\frac{2\pi}{\hbar\omega'}(V^{\ddagger}-E)=\frac{2K(E)}{\hbar}\,. \tag{3.6}$$

The effective frequency ω', which depends on E for a nonlinear barrier, is used to calculate the unstable normal mode frequency $\lambda^{\ddagger}$ defined through the Grote–Hynes equation,[29–31] $\lambda^{\ddagger}=\omega'[1+\hat{\gamma}(\lambda^{\ddagger})/\lambda^{\ddagger}]^{-1/2}$. Finally, $T(E)$ is taken as the transmission probability for an unstable normal mode with energy E and frequency $\lambda^{\ddagger}$,

$$T(E)=\left\{1+\exp\left[\frac{2\pi(V^{\ddagger}-E)}{\hbar\lambda^{\ddagger}}\right]\right\}^{-1}=\left\{1+\exp\left[\frac{2K(E)\omega'}{\hbar\lambda^{\ddagger}}\right]\right\}^{-1}. \tag{3.7}$$

For a parabolic barrier, this formula for $T(E)$ reduces to $T(E)$ for the unstable barrier top normal mode.[49]

D. Semiclassical reactive flux

For large barriers, first passage time simulations are inefficient: the mean waiting time for a particle to escape a well grows exponentially with the barrier height. Reactive flux methods circumvent the waiting time by starting particles from the top of a barrier and averaging certain time correlation functions over the resulting trajectories.[3–8] Here we generalize the reactive flux technique to include semiclassical tunneling. We will see that tunneling softens a classical step function to the semiclassical transmission probability $T(E)$.

The average of an observable $\hat{O}$ which depends on the trajectory $\{q(t),p(t)\}$ is

$$\langle \hat{O} \rangle = (2\pi\hbar Q)^{-1} \int dq \int dp e^{-\beta E(q,p)} \langle \hat{O} \rangle_R , \tag{3.8}$$

with $E(q,p)=p^2/2m+V(q)$ and $Q=(2\pi\hbar)^{-1}\int dq \int dp \times \exp[-\beta E]$. The observable is then averaged over random force histories $R(t)$ which generate semiclassical dynamics trajectories $\{q(t),p(t)\}$ starting from the initial (q,p). We eliminate the variable p in favor of E. The Jacobian of the transformation from (q,p) to (q,E) is m/p, and

$$\langle \hat{O} \rangle = (2\pi\hbar Q)^{-1} \int_{-\infty}^{\infty} dq \int_{V(q)}^{\infty} dE e^{-\beta E} \times \frac{m}{p(q,E)} \{ \langle \hat{O}(q,p) \rangle_R + \langle \hat{O}(q,-p) \rangle_R \}. \tag{3.9}$$

The momentum $p(q,E)$ is now a function of q and E, and is defined as the positive branch of $\sqrt{2m[E-V(q)]}$. Two types of trajectories contribute to $\langle \hat{O} \rangle$ for each value of (q,E). Trajectories contributing to $\hat{O}(q,p)$ start at q with positive momentum p; those counted in $\hat{O}(q,-p)$, start at q with negative momentum. These two sets of trajectories must also be averaged over histories of the random force.

We specialize to the reactive flux operator $\hat{k}_{A\to B}(t)$ for a generic bistable system with states A and B,

$$\hat{k}_{A\to B}(t) = -\frac{Q}{Q_A} \left\{ \frac{d}{dt} \Theta_A[q,E] \right\} \Theta_B[q(t),E(t)]. \tag{3.10}$$

The ratio of partition functions Q_A/Q is $\langle \Theta_A \rangle$. The characteristic function $\Theta_A(q,E)$ is 1 when coordinate q is in the classically allowed region defined as state A and 0 otherwise. In general, one can define $\Theta_A(q,E)=\Theta[S_A(q,E)]$, where the surface function $S_A(q,E)$ is positive for (q,E) in a classically allowed region of state A, negative for (q,E) outside of state A, and zero on the border. The characteristic function $\Theta_B(q,E)$ is defined analogously. Since q must be in either state A or state B for classically allowed energies, $\Theta_A(q,E)+\Theta_B(q,E)=\Theta[E-V(q)]$. The unsubscripted Θ is the Heaviside function.

The time derivative of Θ_A is

$$\frac{d}{dt} \Theta_A(q,E) = \frac{\partial \Theta_A}{\partial q} \frac{dq}{dt} + \frac{\partial \Theta_A}{\partial E} \frac{dE}{dt} . \tag{3.11}$$

The time derivative dE/dt is of $\mathcal{O}(\sqrt{\gamma})$; since we are concerned with the weak damping limit of small γ we can safely neglect the second term in Eq. (3.11). Using the notation of Ref. 9, the first term may be written

$$\dot{\Theta}_A(q,E) = \delta[S_A(q,E)] \nabla_q S_A \dot{q} = -\delta_A(q,E) v_A . \tag{3.12}$$

The velocity v_A is normal to the dividing surface and positive when exiting state A, $v_A = -\dot{q} \cdot \nabla_q S_A / |\nabla_q S_A|$, and $\delta_A(q,E)=\delta[S_A(q,E)]|\nabla_q S_A|$.

For a one-dimensional potential, one can define state A as the classically allowed region between left and right boundaries $q^{\star}_{A,l}$ and $q^{\star}_{A,r}$. Assuming that $E=V(q)$ at most twice in the region so that left and right turning points are unambiguous,

$$\Theta_A(q,E) = \Theta[q_{A,r}(E)-q] - \Theta[q-q_{A,l}(E)]. \tag{3.13}$$

For $E \geqslant V(q^{\star}_{A,r})$, $q_{A,r}(E)=q^{\star}_{A,r}$. For $E<V(q^{\star}_{A,r})$, $q_{A,r}(E)$ is the location of the right turning point for motion in state A: $V[q_{A,r}(E)]=E$. On the left side of state A, $q_{A,l}(E)$ is defined as $q^{\star}_{A,l}$ for energies above $V(q^{\star}_{A,l})$, and as the left turning point otherwise. If E is smaller than the minimum of the potential in state A, then E is not allowed classically and $\Theta_A(q,E)=0$.

The definition of $\hat{k}_{A\to B}(t)$ is inserted into Eq. 3.9 to give

$$k_{A\to B}(t) \equiv \langle \hat{k}_{A\to B}(t) \rangle = (2\pi\hbar Q_A)^{-1} \int_{E_A}^{\infty} dE \int dq \, \delta_A(q,E) \times \langle \Theta_B(t|q,p_B) - \Theta_B(t|q,p_A) \rangle_R . \tag{3.14}$$

The energy integral has been restricted to values larger than E_A, the minimum classically allowed energy in state A. The absolute value of the velocity v_A normal to the dividing surface has been identified with $p(q,E)/m$. The momentum p_B points into state B; the momentum $p_A=-p_B$ points into state A; and p_B and p_A are both equal in magnitude to $p(q,E)$. The characteristic function $\Theta_B(t|q,p)$ is 1 for those trajectories with initial position and momentum (q,p) which are in state B at time t, and 0 otherwise. The function $\delta_A(q,E)$ places the initial q at either a barrier top or a turning point of state A. If q is at a turning point then we consider p_B the outward momentum instantaneously before the turning point, and p_A the inward momentum just after reflection from the turning point at q.

When the initial velocity points out of state A, the probability that a particle will be transmitted to state B is $T(q,E)$. The trajectories contributing to $\Theta_B(t|q,p_B)$ bifurcate,

$$\Theta_B(t|q,p_B) = T(E)\Theta_B(t|q_B,p_B) + [1-T(E)]\Theta_B(t|q_A,p_A). \tag{3.15}$$

The trajectories in the first set, with weight $T(E)$, have have been transmitted into state B. The initial position is now termed q_B. If $E>V(q)$, then $q_B=q$. If $E<V(q)$, the particle has tunneled through the barrier between A and B. The original q is a turning point of energy E on the A side of the barrier; the particle is removed from q and placed at q_B, the turning point of energy E on the state B side of the barrier. Trajectories in the second set, with weight $1-T(E)$, have been reflected back into state A, p_B is reversed to p_A, and q is renamed q_A. Combining Eq. (3.14) with Θ_B from Eq. (3.15), we have

$$k_{A\to B}(t)=(2\pi\hbar Q_A)^{-1}\int_{E_A}^{\infty}dE\int dq \times\exp[-\beta E]\delta_A(q,E)T(q,E) \times\{\langle\Theta_B(t|q_B,p_B)\rangle_R-\langle\Theta_B(t|q_A,p_A)\rangle_R\} =(2\pi\hbar Q_A)^{-1}\int_{E_A}^{\infty}dE\ \exp[-\beta E]T(E) \times\langle\Theta_B(t|q_B,p_B)\rangle_R-(2\pi\hbar Q_A)^{-1}\int_{E_A}^{\infty}dE \times\exp[-\beta E]T(E)\langle\Theta_B(t|q_A,p_A)\rangle_R. \quad (3.16)$$

To simplify the equation, we have assumed that each energy E corresponds to a single pair of initial conditions (q_B,p_B) and (q_A,p_A) on the B and A sides of the barrier. For energies larger than the barrier height $V^{\ddagger}=V(q^{\ddagger})$, $q_B=q_A=q^{\ddagger}$; otherwise, q_B and q_A are turning points. This formula reduces to the standard reactive flux sampling scheme for classical dynamics as $T(E)$ goes to the classical form $T(E)=\Theta[E-V^{\ddagger}]$.

The initial rate from A to B is the transition state theory estimate, $k_{A\to B}^{\mathrm{TST}}$. At time $t=0$, $\Theta_B(0|q_A,p_A)=0$, and

$$k_{A\to B}^{\mathrm{TST}}\equiv\lim_{t\to 0^+}k_{A\to B}(t)=(2\pi\hbar Q_A)^{-1}\int_{E_A}^{\infty}dE \times\exp[-\beta E]T(E). \quad (3.17)$$

This thermal average of $T(E)$ can be used to obtain a correction factor Λ for the harmonic barrier Ξ from Eq. (2.5).[31] This correction factor is obtained from the Grote–Hynes barrier frequency $\lambda^{\ddagger}$ and the ratio of the quantum TST rate to the classical TST rate, $k_{A\to B}^{\mathrm{TST,cl}}$. The classical rate is obtained using $T(E)=\Theta(E-V^{\ddagger})$ in Eq. 3.17. The correction factor Λ is

$$\Lambda=\frac{\sin(\beta\hbar\lambda^{\ddagger}/2)}{\beta\hbar\lambda^{\ddagger}/2}\,\beta\int_{E_A}^{\infty}dE\ \exp[-\beta(E-V^{\ddagger})]T(E). \quad (3.18)$$

The product $\Lambda\Xi$ is well-behaved even below crossover temperature because Λ corrects for the nonlinearity of the potential and for the finite height of the barrier. In particular, Λ cancels the divergence due to the term $1/\sin(\beta\hbar\lambda^{\ddagger}/2)$ in Ξ.

In simulations, it is convenient to calculate the transmission coefficient $\kappa_{A\to B}$ rather than $k_{A\to B}$ itself,

$$\kappa_{A\to B}(t)\equiv k_{A\to B}(t)/k_{A\to B}^{\mathrm{TST}}. \quad (3.19)$$

The initial energy is chosen from the distribution

$$\rho(E)=\frac{\exp(-\beta E)T(E)\Theta(E-E_A)}{\int_{E_A}^{\infty}dE\exp(-\beta E)T(E)}. \quad (3.20)$$

Choosing M initial values for the energy results in M pairs of trajectories, the μth pair starting with (q_A^{μ},p_A^{μ}) and (q_B^{μ},p_B^{μ}). The transmission coefficient is evaluated as

$$\kappa_{A\to B}(t)=\frac{1}{M}\sum_{\mu=1}^{M}[\Theta_B(t|q_B^{\mu},p_B^{\mu})-\Theta_B(t|q_A^{\mu},p_A^{\mu})]. \quad (3.21)$$

If $\kappa_{A\to B}(t)$ decays slowly for large enough t, the plateau value $\kappa_{A\to B}$ is defined, and the escape rate predicted by the semiclassical reactive flux method is

$$k_{A\to B}=\kappa_{A\to B}\Lambda\Xi k_{A\to B}^{\mathrm{TST,cl}}. \quad (3.22)$$

The classical reactive flux method has been generalized to multistate systems.[9] The same generalizations follow for the semiclassical reactive flux method outlined here for bistable systems. The classical step function at the dividing surface, $\Theta(E-V^{\ddagger})$, is simply replaced by the quantum $T(E)$.

IV. TURNING TRAJECTORIES INTO OBSERVABLES

Armed with the semiclassical simulation methods of Section III, we have computed the escape rate Γ of particles out of a well, the average energy of escaping particles $\langle\epsilon\rangle$, the probability of a correlated hop P_1, the diffusion constant D, the mean square length per jump $\langle l^2\rangle$, and various other quantities. When the barrier height $V^{\ddagger}$ is small, barrier crossings can be frequent, permitting direct sampling of these observables from equilibrium simulations. First passage simulations are described in Section IV A. For large barrier heights, reactive flux methods increase the sampling efficiency. The semiclassical reactive flux correlation functions which we used are presented in Section IV B.

A. First passage simulations

First passage time simulations were used to obtain distributions of energies of escaping particles and distributions of jump lengths. These simulations were performed by starting each trajectory with the particle in well 0 of the periodic cosine potential. Each trajectory was continued until the particle escaped from well 0, either by passing over the barrier or by tunneling through the barrier. At this point, the energy of the particle was stored to accumulate $f(\epsilon)$, the distribution of energies of particles crossing the barrier. Each trajectory was continued from this point until the particle experienced its first turning point after escape. A turning point over well n defines the length of the first correlated segment of the jump as $|n|$. Averaging over many trajectories gives $P(n)$, the distribution of lengths for the correlated segments which compose a jump.

At first, we selected the initial energy of each particle from a Boltzmann distribution in well 0. When the friction was small, however, we found that the small Boltzmann tail extending above the barrier skewed the distributions $f(\epsilon)$ and $P(n)$. Furthermore, these energetic trajectories do not correspond to reactive flux out of well 0: when integrated backwards in time they usually leave well 0 immediately. The presence of these trajectories is essentially a finite barrier height effect, since their numbers decrease exponentially with increasing barrier height. When friction was small,

$\delta \lesssim 1$, we removed these energetic trajectories from our sampling by giving each trajectory an initial energy of 1 k_BT above the minimum in well 0.

B. Reactive flux correlation functions

Due to the symmetry of the periodic potential, all the required reactive flux correlation functions can be expressed in terms of trajectories which are transmitted from well 0 to well 1 at time $t=0$. The initial distribution of energies and positions, termed $\rho_0^+(q,E)$, is

$$\rho_0^+(q,E)=\frac{\exp(-\beta E)T(E)\delta_0(q,E)\Theta(E)}{\int_0^\infty dE\int_{l_0/2}^{l_0}dq\ \exp(-\beta E)T(E)\delta_0(q,E)}. \tag{4.1}$$

The symbol "+" is a reminder that the initial direction of motion is into well 1; i.e., the initial momentum is the nonnegative root $\sqrt{2m[E-V(q)]}$. The minimum of the potential is at 0 and the barrier energy is $V^\ddagger$. For $E<V^\ddagger$, $\delta_0(q,E)$ places q at the left turning point at energy E in well 1. For $E\geqslant V^\ddagger$, $\delta_0(q,E)$ places q at the barrier top between well 0 and well 1, $q=l_0/2$. The transmission probability $T(E)$ is calculated for the cosine barrier and corrected for friction according to Eq. (3.7).

The escape rate from well 0 to well n can be written as

$$k_{0\to n}=\kappa_{0\to n}\Gamma_{\mathrm{TST}}, \tag{4.2}$$

where Γ_{TST} is the transition state theory value $(\omega/\pi)\exp(-\beta V^\ddagger)\Lambda\Xi$. The well frequency is ω; the nonlinear, finite barrier height correction Λ is defined by Eq. (3.18). Now we select M initial values for E and the corresponding M values for q from the distribution $\rho_0^+(q,E)$. The initial energy of the μth trajectory is E_μ. The stochastic semiclassical dynamics generates M trajectories; the position of the particle at time t for the μth trajectory is $q_\mu(t)$. The transmission coefficient $\kappa_{0\to n}$ is given by the plateau value of $\kappa_{0\to n}(t)$,

$$\kappa_{0\to n}(t)=\frac{1}{2M}\sum_{\mu=1}^{M}\Theta_n[q_\mu(t)]-\Theta_{n+1}[q_\mu(t)] +\Theta_{-n}[q_\mu(t)]-\Theta_{-n+1}[q_\mu(t)]. \tag{4.3}$$

In order to maintain the symmetry between n and $-n$ while using the distribution ρ_0^+, we have replaced the rate $k_{0\to n}$ by the equivalent $(k_{0\to n}+k_{0\to -n})/2$ before averaging over trajectories.

The total escape rate Γ is $\Sigma_{n\neq 0}k_{0\to n}$, which can be rewritten as $\Gamma=\kappa_{0\to}\Gamma_{\mathrm{TST}}$. The transmission coefficient $\kappa_{0\to}$ is the plateau value of a time correlation function,

$$\kappa_{0\to}(t)=\sum_{n\neq 0}\kappa_{0\to n}(t). \tag{4.4}$$

Noting that $\Sigma_{n\neq 0}\Theta_n(q)=1-\Theta_0(q)$, we have in terms of the M trajectories

$$\kappa_{0\to}(t)=\frac{1}{M}\sum_{\mu=1}^{M}\Theta_1[q_\mu(t)]-\Theta_0[q_\mu(t)]. \tag{4.5}$$

The average energy of escaping particles is defined through the time-dependent quantity $\langle\epsilon(t)\rangle$,

$$\langle\epsilon(t)\rangle=[\kappa_{0\to}(t)]^{-1}\frac{1}{M}\sum_{\mu=1}^{M}\{\Theta_1[q_\mu(t)]-\Theta_0[q_\mu(t)]\} \times(E_\mu-V^\ddagger)/k_BT. \tag{4.6}$$

The energy being averaged, $E_\mu-V^\ddagger$, is the initial energy of the μth particle (rather than the energy at time t) relative to the barrier energy. As the particles dissipate energy and become trapped, $\langle\epsilon(t)\rangle$ approaches the plateau value $\langle\epsilon\rangle$.

The diffusion constant is defined as

$$D=\frac{1}{2}\Gamma\langle l^2\rangle=\frac{1}{2}\sum_n k_{0\to n}(nl_0)^2. \tag{4.7}$$

It is convenient to redefine D as $D=\tilde{D}D_{\mathrm{TST}}$. The transition state value for the diffusion constant is

$$D_{\mathrm{TST}}=\tfrac{1}{2}\Gamma_{\mathrm{TST}}l_0^2, \tag{4.8}$$

i.e. particles escape with the transition state rate and hop only a single lattice spacing. In terms of the state-to-state reactive flux transmission coefficients, $\tilde{D}$ is the plateau value of $\tilde{D}(t)$,

$$\tilde{D}(t)=\sum_n \kappa_{0\to n}(t)n^2. \tag{4.9}$$

In terms of the M trajectories,

$$\tilde{D}(t)=\frac{1}{M}\sum_{\mu=1}^{M}\sum_n (2n-1)\Theta_n[q_\mu(t)]. \tag{4.10}$$

Finally, comparing expressions for D and $\kappa_{0\to}$, it is evident that

$$\langle(l/l_0)^2\rangle=\tilde{D}/\kappa_{0\to}. \tag{4.11}$$

Reactive flux methods require the existence of a plateau time with slow exponential decay. We have verified that we have reached such a regime for the simulation results we report.

V. RESULTS

We have performed Langevin dynamics simulations for the motion of a particle of mass m on the cosine surface

$$V(q)=(V^\ddagger/2)[1-\cos(2\pi q/l_0)]. \tag{5.1}$$

The nth well is defined as $(n-1/2)l_0<q<(n+1/2)l_0$. The frequency $\omega=(2\pi/l_0)\sqrt{V^\ddagger/2m}$. In the classical limit, the reduced frequency $\beta\hbar\omega\to 0$. The crossover transition from activated escape to deep tunneling is approximately $\beta\hbar\omega=2\pi$. Unless noted otherwise, we used a barrier height of 5 k_BT for $\beta\hbar\omega=0$ and 0.2π, and a barrier height of 25 k_BT for $\beta\hbar\omega=\pi$, 1.8π, and 3π. We compare simulation results with theoretical results except for the largest frequency, $\beta\hbar\omega=3\pi$, where the theory does not converge.

The value of the static friction γ was defined through the energy loss parameter δ from Eq. (A17), $\gamma\equiv\delta\omega/4\beta V^\ddagger$. The Langevin equation was integrated directly for $\delta\geqslant 1$; the en-

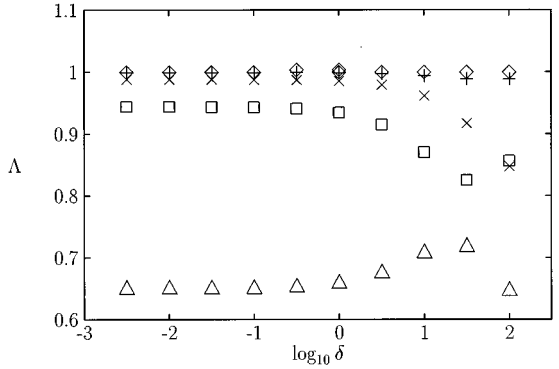

FIG. 1. The correction factor Λ for the parabolic barrier quantum factor Ξ is shown as a function of the energy loss parameter δ. $\diamond$: $\beta\hbar\omega=0$, $\beta V^{\ddagger}=5$; $+$: $\beta\hbar\omega=0.2\pi$, $\beta V^{\ddagger}=5$; $\square$: $\beta\hbar\omega=\pi$, $\beta V^{\ddagger}=5$; $\times$: $\beta\hbar\omega=\pi$, $\beta V^{\ddagger}=25$; $\triangle$: $\beta\hbar\omega=1.8\pi$, $\beta V^{\ddagger}=25$.

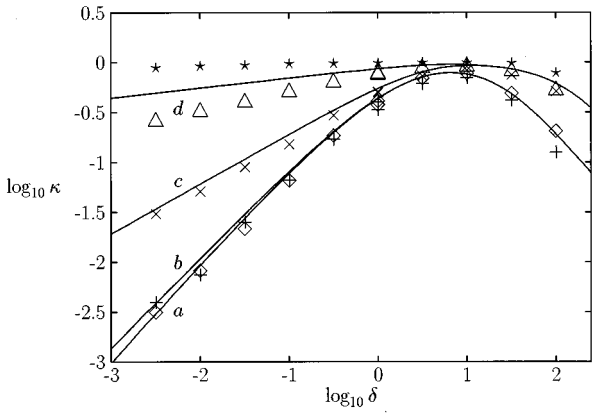

FIG. 2. The transmission coefficient κ from is shown as a function of the energy loss parameter δ. Points are reactive flux simulations; lines a–d are theory. $\diamond$ and a: $\beta\hbar\omega=0,\beta V^{\ddagger}=5$; $+$ and b: $\beta\hbar\omega=0.2\pi,\beta V^{\ddagger}=5$; $\times$ and c: $\beta\hbar\omega=\pi,\beta V^{\ddagger}=25$; $\triangle$ and d: $\beta\hbar\omega=1.8\pi,\beta V^{\ddagger}=25$; $\bigstar$: $\beta\hbar\omega=3\pi,\beta V^{\ddagger}=25$. The theoretical estimate is $\kappa=\Upsilon\lambda^{\ddagger}/\omega$. Simulation error bars are smaller than the size of the points.

ergy space method was used for $\delta\leqslant 1$. As shown below, results from the two methods agree well at $\delta=1$.

A. Λ

As discussed in Section III D, Λ is the ratio of the thermally weighted semiclassical transmission probability for the cosine potential to the transmission probability for a harmonic barrier with frequency given by the unstable barrier top normal mode. This ratio is unity when a harmonic approximation suffices for the quantum effects of tunneling and reflection. The values we obtain for Λ are presented in Fig. 1. In the strong damping region, when the barrier height is large enough, the steepest descent, parabolic barrier estimate is good. One finds that Λ is almost unity in this region. For finite barrier heights and weaker damping, the true rate will be smaller than the rate estimated from a parabolic barrier because the nonlinear nature of the cosine potential implies a larger imaginary action through the barrier and hence a smaller transmission coefficient. The fact that Λ goes substantially below unity in the strong damping region is qualitatively correct, though our results are not quantitative because the barrier is after all not separable.

For the classical frequency $\beta\hbar\omega=0$, plotted with the $\diamond$ symbol, $\Lambda=1$ by definition. The steepest descent estimate is accurate for the next larger frequency, $\beta\hbar\omega=0.2\pi$. As shown with the $+$ symbol, Λ deviates very little from 1 throughout the entire range of damping.

When the bare frequency $\beta\hbar\omega$ is increased to π, the harmonic approximation predicts a larger tunneling factor than we estimate for the nonlinear cosine barrier. The symbol $\square$ represents results for $\beta\hbar\omega=\pi$ and the barrier height $V^{\ddagger}=5k_BT$. For weak damping, Λ drops below 1 due to the finite height of the nonlinear barrier. At moderate to strong damping, tunneling is less important and we would expect Λ to approach 1. Instead, it decreases further, indicating that our method for obtaining $T(E)$ which assumes separability of effective barrier modes is not valid for strong friction. The finite barrier height effects for weak friction are reduced when $V^{\ddagger}$ is increased to 25 k_BT, with $\beta\hbar\omega$ still equal to π. For this larger barrier height, Λ as shown with the $\times$ symbol is again close to 1. Nonlinearities in the cosine potential are now below the energies important for escaping particles.

When $\beta\hbar\omega$ is increased to 1.8π with $\beta V^{\ddagger}=25$, just above the crossover temperature and plotted with $\triangle$, the correction factor Λ is roughly 0.65 for underdamped escape, indicating that a harmonic approximation again overestimates the tunneling enhancement to the rate at low friction. Just as with $\beta\hbar\omega=\pi$, the deviation of Λ from unity for $\beta\hbar\omega=1.8\pi$ and large damping are likely due to the failure of the corrected $T(E)$ to adequately describe the effects of friction. For weak friction, however, Λ has attained a plateau value and the frictional correction to $T(E)$ is very minor. Since we are concerned here with weak friction, not strong friction, we do not address how $T(E)$ can be improved in the large friction regime.

B. κ

The transmission coefficient for escape from well 0, $\kappa\equiv\kappa_{0\rightarrow}$, is shown in Fig 2. The simulation results were obtained using the reactive flux method; the theoretical estimate is $\kappa=\Upsilon\lambda^{\ddagger}/\omega$. For the reduced frequency $\beta\hbar\omega=0$ (classical dynamics) the theory and simulation agree perfectly.

The simulation results for $\beta\hbar\omega=0.2\pi$ are also in good agreement with the theoretical prediction for κ. A small discrepancy is noticeable only at the largest value of the friction, $\delta=100$. At this large friction, the simulation results are probably in error. The semiclassical dynamics method allows tunneling each time the particle reaches a turning point, rather than only when the unstable barrier top normal mode experiences a turning point. Tunneling serves to increase the chance that a particle in well 1 will return to well 0, and κ from the simulation is smaller than the correct result.

For the next larger frequency, $\beta\hbar\omega=\pi$, the agreement between theory and simulation is quite good, although the theoretical prediction for κ consistently overestimates the simulation results. The theory we use also predicts too large

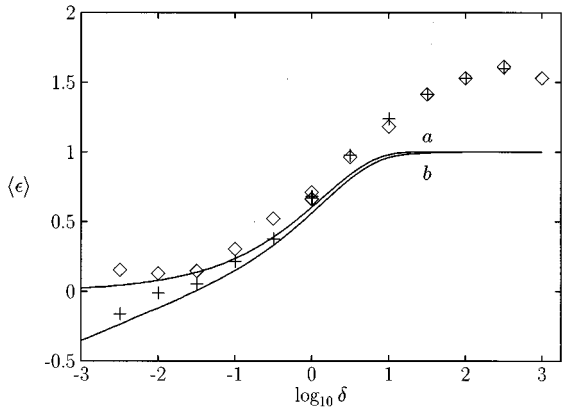

FIG. 3. The average energy of escaping particles relative to the barrier energy in units of k_BT, $\langle\epsilon\rangle=\beta\langle E-V(l_0/2)\rangle$, is shown as a function of the energy loss parameter δ. Points are reactive flux simulations; lines a–b are theory. $\diamond$ and a: $\beta\hbar\omega=0,\beta V^{\ddagger}=5$; $+$ and b: $\beta\hbar\omega=0.2\pi,\beta V^{\ddagger}=5$.

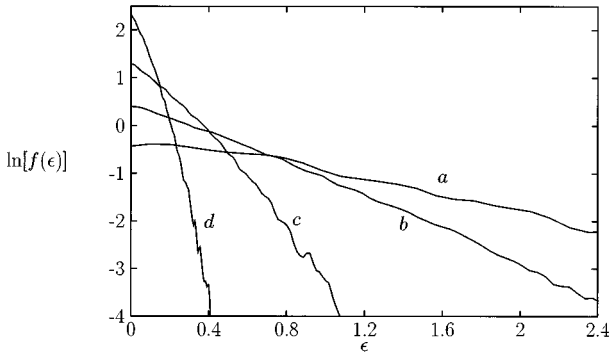

FIG. 4. The distribution of energies $f(\epsilon)$ of escaping particles is shown as a function of the difference ϵ from the barrier energy in units of k_BT. Results are from mean first passage simulations with $V^{\ddagger}=5k_BT$ and $\beta\hbar\omega=0$. The four lines correspond to four choices for the energy loss parameter δ: a, $\delta=10$; b, $\delta=1$; c, $\delta=0.1$; d, $\delta=0.01$.

a value for κ at $\beta\hbar\omega=1.8\pi$. The difference between theory and simulation is especially noticeable for small friction, where our semiclassical dynamics method should be accurate. We ascribe the difference to the finite height and the nonlinearity of the barrier in the simulations. First, the energy loss δ at the barrier top energy is larger than δ at the energies important for tunneling. Since the escape rate scales as δ in the underdamped regime, the escape rate from theory is too large. Second, since $T(E)$ decreases faster for the cosine potential than for a parabolic barrier, escape at a lower energy is more classical-like in the simulation than in the theory. Again, this causes κ to be smaller than the theoretical prediction based on a parabolic barrier.

The qualitative prediction of the theory, $\kappa\approx\delta^{1-\beta\hbar\omega^{\ddagger}/2\pi}$ for low friction, is correct, but can only be used to predict escape rates for barriers with $\beta\hbar\omega\leqslant 2\pi$, i.e. above the crossover temperature. According to this expression, $\kappa\rightarrow 1$ as $\beta\hbar\omega$ approaches 2π from below. Simulations with $\beta\hbar\omega=3\pi$ indicate that κ is essentially 1 below the crossover temperature.

C. $\langle\epsilon\rangle$ and $f(\epsilon)$

One measure of the importance of frictional forces and tunneling is $\epsilon\equiv(E-V^{\ddagger})/k_BT$, the energy of an escaping particle relative to the barrier top energy. The average energy of escaping particles $\langle\epsilon\rangle$ is displayed in Fig. 3 for the two smallest frequencies, $\beta\hbar\omega=0$ and $0.2\ \pi$. At small damping, $\delta\lesssim 1$, the simulation and theory agree. As predicted by theory, the energy of a classical particle escaping from a well scales as $0.82\sqrt{\delta}$. The escape energies at low friction also agree for the nearly classical barrier frequency $\beta\hbar\omega=0.2\pi$.

At moderate to large damping, however, there is a clear difference between the simulation result and the theoretical prediction that $\langle\epsilon\rangle\rightarrow 1$. The difference stems from the fact that the energy in the theory is that of the unstable normal mode, whereas the energy in the simulation refers to the energy in the reaction coordinate. One can show, however, that in the moderate to large damping limit ($\delta>1$ and $\Upsilon\approx 1$),

$$\langle\epsilon\rangle=1+\frac{1}{2}\ \frac{\hat{\gamma}(\lambda^{\ddagger})\lambda^{\ddagger}}{\omega^2}\ , \tag{5.2}$$

where ϵ refers to the reaction coordinate energy.[50] When friction becomes large, $\lambda^{\ddagger}\approx\omega^2/\hat{\gamma}(\lambda^{\ddagger})$, and $\langle\epsilon\rangle\rightarrow(3/2)k_BT$. Within simulation error bars, roughly the size of the points in Fig. 3, the average energy of classical escaping particles in the large friction regime is indeed $(3/2)k_BT$.

The shift to smaller escape energies for the classical particle leads to a narrowing of the distribution of escape energies, $f(\epsilon)$. This distribution is peaked very strongly at the barrier top energy as the friction becomes smaller. The distribution of escape energies $f(\epsilon)$ from first passage simulations, normalized to 1, is shown in Fig. 4 as a function of ϵ for escape of classical particles from one well of the cosine surface. Results are shown for four values of the energy loss parameter δ. When $\delta\gtrsim 1$, the form of $f(\epsilon)$ is

$$f(\epsilon)\approx\kappa^{-1}\ \exp(-\epsilon)\,\mathrm{erf}\sqrt{\epsilon\lambda^{\ddagger}/\hat{\gamma}(\lambda^{\ddagger})}. \tag{5.3}$$

In the underdamped regime, $\delta\lesssim 1$,

$$f(\epsilon)\approx(0.82\delta)^{-1/2}\ \exp[-\epsilon/0.82\delta^{1/2}]. \tag{5.4}$$

The distribution $f(\epsilon)$ clearly collapses toward 0 as friction is decreased in the simulations. Furthermore, the decay of $f(\epsilon)$ is very close to exponential in all cases. The agreement of the moment $\langle\epsilon\rangle$ given by theory and simulation indicates that the decay constants as given by theory and simulation also agree.

Results for escape energies for all barrier frequencies are shown in Fig. 5. For the smallest two frequencies the barrier height was 5 k_BT; for the remaining frequencies, it was 25 k_BT. Since the results for $\beta\hbar\omega=0$ and 0.2π have been discussed above, we concentrate now on $\beta\hbar\omega=\pi$, 1.8π, and 3π. When $\beta\hbar\omega=\pi$, the agreement between theory and simulation is quite good. As friction is decreased, tunneling becomes more important and occurs at lower and lower energies. In Fig. 6 we show the distribution of energies $f(\epsilon)$

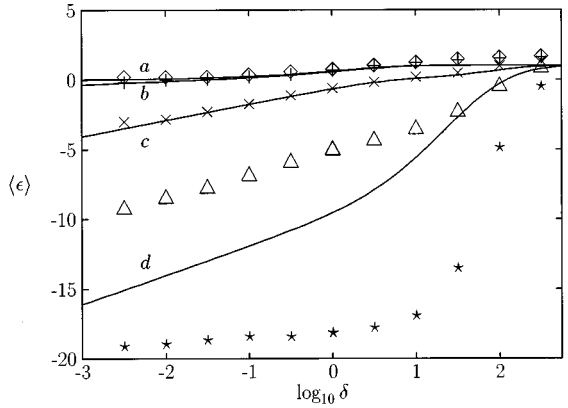

FIG. 5. The average energy of escaping particles relative to the barrier energy in units of k_BT, $\langle\epsilon\rangle=\beta\langle E-V(l_0/2)\rangle$, is shown as a function of the energy loss parameter δ. Points are reactive flux simulations; lines a–d are theory. $\diamond$ and a: $\beta\hbar\omega=0,\beta V^{\ddagger}=5$; $+$ and b: $\beta\hbar\omega=0.2\pi,\beta V^{\ddagger}=5$; $\times$ and c: $\beta\hbar\omega=\pi,\beta V^{\ddagger}=25$; $\triangle$ and d: $\beta\hbar\omega=1.8\pi,\beta V^{\ddagger}=25$; $\bigstar$: $\beta\hbar\omega=3\pi,\beta V^{\ddagger}=25$. Simulation error bars are smaller than the size of the points.

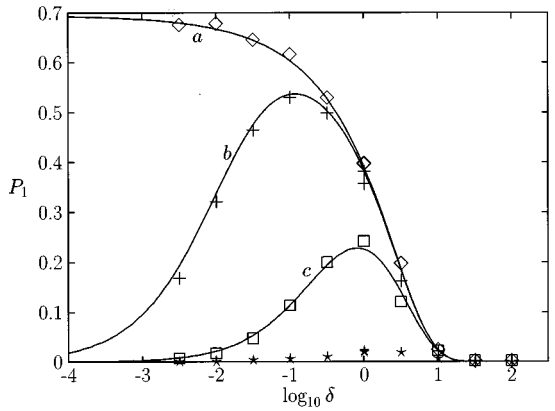

FIG. 7. The correlated hop probability P_1 is shown as a function of the energy loss parameter δ for various values of the quantum parameter $\beta\hbar\omega$. Lines are theory; points are results from first passage simulations with $\beta V^{\ddagger}=5$. $\diamond$ and a: $\beta\hbar\omega=0$; $+$ and b: $\beta\hbar\omega=0.2\pi$; $\square$ and c: $\beta\hbar\omega=\pi$; $\bigstar$: $\beta\hbar\omega=3\pi$.

obtained from first passage simulations with $\beta\hbar\omega=\pi$ and a barrier height of 5 k_BT. For the largest friction, $\delta=100$, most of the particles are activated and escape at energies above the barrier energy. As the friction is decreased, the distribution shifts to lower energies and tunneling dominates the escape.

Results for $\beta\hbar\omega=1.8\pi$ in Fig. 5 show a discrepancy in $\langle\epsilon\rangle$ from theory and simulation. The theory predicts escape energies about 5 k_BT lower than those seen in simulation. This difference is due to nonlinearities in the cosine potential. Since $T(E)$ decreases faster for the cosine potential than for a harmonic potential, tunneling occurs at a higher energy than predicted by theory. When friction is large, tunneling particles escape near the top of the barrier, nonlinearity of the barrier is not important, and the theoretical results and simulation results agree.

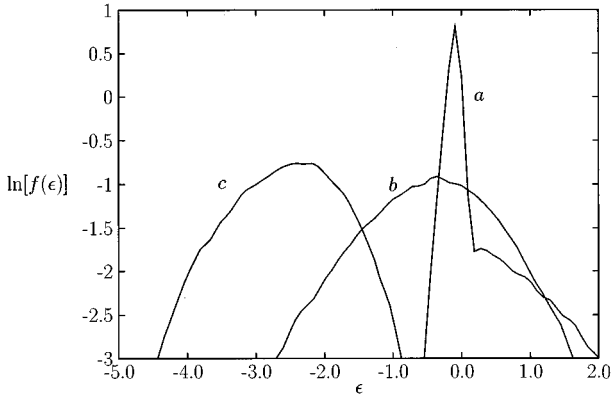

FIG. 6. The distribution of energies $f(\epsilon)$ of escaping particles is shown as a function of the difference ϵ from the barrier energy in units of k_BT. Results are from mean first passage simulations with $V^{\ddagger}=5k_BT$ and $\beta\hbar\omega=\pi$. The three lines correspond to three choices for the energy loss parameter δ: a, $\delta=100$; b, $\delta=1$; c, $\delta=0.01$.

For the largest frequency, $\beta\hbar\omega=3\pi$, corresponding to a temperature below crossover, it is clear that escape is due to tunneling from deep in the well for all but the strongest values of the friction. A thorough investigation of escape in this regime requires a more complete quantum mechanical treatment than is provided by the semiclassical dynamics algorithm. Although we have not included the effects of quantization of energy levels in the simulation, we expect the qualitative picture presented here is valid.

D. P_1

The correlated hop probabilities P_1 as measured from first passage simulations are shown in Fig. 7. This is the probability that a particle escaping from a well will traverse at least one other well before suffering a reversal in its velocity. It characterizes the probability that a segment of the trajectory of an activated particle will include a correlated hop over several lattice spacings. The barrier height used in these simulations was 5 k_BT, except for $\beta\hbar\omega=3\pi$ where the barrier height was 10 k_BT. As in all the figures, two points are plotted for $\delta=1$, one from the energy space simulation and one from the Langevin simulation. A small difference is noticeable between the values for P_1 from the two simulations; this difference is roughly the size of the simulation uncertainty.

When friction is large, the probability of a correlated hop is small. As the friction decreases, P_1 rises for classical escape, saturating at a value of almost 0.7. A plateau is reached because the root mean square energy fluctuation in going from barrier to barrier is on the order of the energy of the escaping particle: both are proportional to $\sqrt{\delta}$.

When tunneling is allowed, however, P_1 eventually falls with decreasing friction. The reason is that a greater number of particles escape by tunneling when friction becomes smaller, the tunneling energy decreases, and the probability to tunnel across two barriers decreases. The agreement between theory and simulation is quite good; effects due to

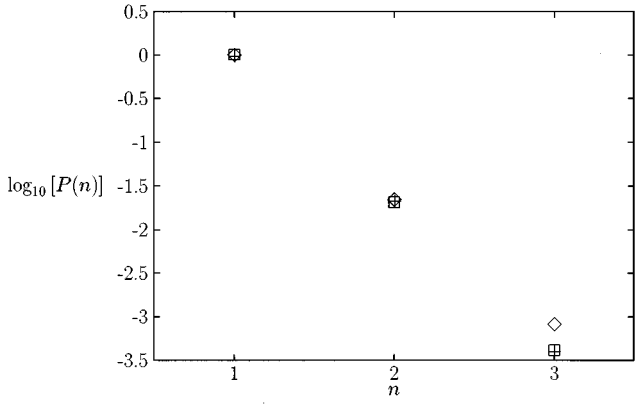

FIG. 8. The probability $P(n)$ that a particle escaping from well 0 suffers its first reversal of velocity while over well n is depicted for three values of the parameter $\beta\hbar\omega$: $\diamond, \beta\hbar\omega=0$; $+, \beta\hbar\omega=0.2\pi$; $\square, \beta\hbar\omega=\pi$. For all cases $V^{\ddagger}=5k_BT$ and $\delta=10$.

finite barrier heights do not seem to affect P_1 for the parameters we consider.

The simulations for $\beta\hbar\omega=3\pi$ indicate the behavior in the deep tunneling regime below the crossover temperature. In this regime, the theory for P_1 no longer converges. Simulations demonstrate that $P_1\approx 0$ when escape is due to ground-state dominated tunneling.

E. $P(n)$

The distribution of jump lengths $P(n)$ is another indication of the probability of a long correlated hop. Calculated in first passage simulations, $P(n)$ is the probability that a particle escaping from well 0 will suffer its first reversal of velocity while traveling over well n. The normalization condition is $\Sigma_{n=1}^{\infty}P(n)=1$, and the probability of a correlated hop P_1 is $1-P(1)$. Results for $P(n)$ from first passage simulations with $V^{\ddagger}=5k_BT$ and $\beta\hbar\omega=0$, 0.2π, and π are shown in Figs. 8–11. For these simulations, the initial energy of the particle was 1 k_BT above the bottom of the well.

In Fig. 8 the energy loss parameter $\delta=10$. All of the hops were 3 lattice spacings or less, and the difference between $P(n)$ for the three values of $\beta\hbar\omega$ is insignificant. Furthermore, $P(n)$ decays exponentially with increasing n,

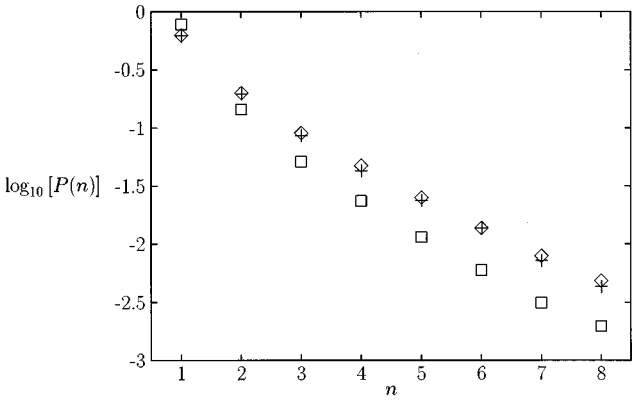

FIG. 9. Same as Fig. 8, but with $\delta=1$.

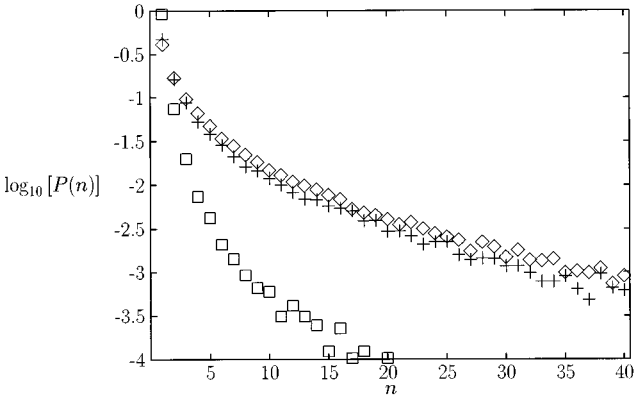

FIG. 10. Same as Fig. 8, but with $\delta=0.1$.

and the geometric series $P(n)=(1-P_1)(P_1)^{n-1}$ is a good approximation to $P(n)$. Next, in Fig. 9, results are shown for $\delta=1$. The jump distributions for $\beta\hbar\omega=0$ and 0.2π are similar and generally larger than $P(n)$ for $\beta\hbar\omega=\pi$. Furthermore, the decay of $P(n)$ is now slower than exponential. The nonexponential decay of $P(n)$ is even more evident in Fig. 10, with $\delta=0.1$. The distribution $P(n)$ is similar for $\beta\hbar\omega=0$ and 0.2π. Tunneling has become important for $\beta\hbar\omega=\pi$, and $P(n)$ decays more quickly than for the lower two frequencies. Results for the smallest value of δ, 0.01, are shown in Fig. 11. Classical dynamics produce a $P(n)$ with an extremely long tail. Tunneling becomes important for escape with $\beta\hbar\omega=0.2$, and $P(n)$ is smaller than for classical escape. Furthermore, for $\beta\hbar\omega=\pi$, $P(n)$ decays much more quickly for $\delta=0.01$ than it did with stronger friction, $\delta=0.1$. As tunneling becomes more important, the distribution of jump lengths shifts to smaller values and becomes exponential once again.

F. D

The ratio $D/D_{\mathrm{TST}}^{\mathrm{cl}}$ of the diffusion constant to the classical transition state theory estimate, $D_{\mathrm{TST}}^{\mathrm{cl}}=(\omega/\pi)l_0^2\exp(-\beta V^{\ddagger})$, is displayed in Fig. 12. These results are from reactive flux calculations. For moderate to large damping, the diffusion constant increases with the quantum

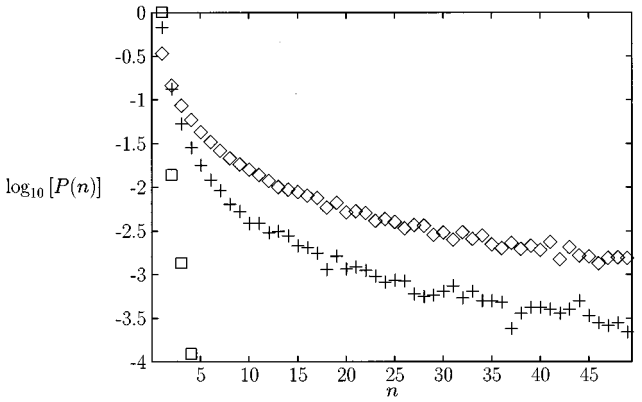

FIG. 11. Same as Fig. 8, but with $\delta=0.01$.

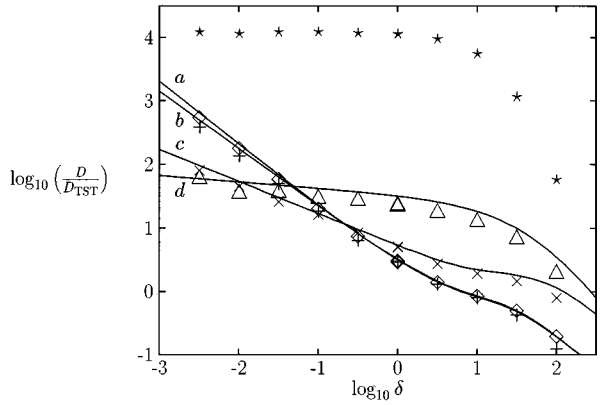

FIG. 12. The diffusion constant D, normalized by the classical transition state theory value $D_{TST}=(\omega/\pi)\exp(-\beta V^{\ddagger})$, is shown as a function of the energy loss parameter δ for various values of the quantum parameter $\beta\hbar\omega$. Points are results from reactive flux simulations, lines are theory. $\diamond$ and a: $\beta\hbar\omega=0$; $+$ and b: $\beta\hbar\omega=0.2\pi$; $\times$ and c: $\beta\hbar\omega=\pi$; $\triangle$ and d: $\beta\hbar\omega=1.8\pi$; $\bigstar$: $\beta\hbar\omega=3\pi$. For $\beta\hbar\omega=0$ and 0.2π, the simulations used $V^{\ddagger}=5k_BT$; for $\beta\hbar\omega=\pi$, 1.8π, and 3π, $V^{\ddagger}=25k_BT$.

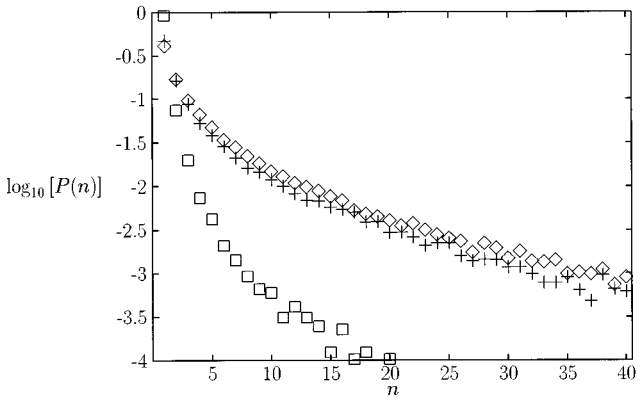

FIG. 13. The mean square lattice spacings per jump $\langle(l/l_0)^2\rangle$, are shown as a function of the energy loss parameter δ for various values of the quantum parameter $\beta\hbar\omega$. Points are results from reactive flux simulations, lines are theory. $\diamond$ and a: $\beta\hbar\omega=0$; $+$ and b: $\beta\hbar\omega=0.2\pi$; $\times$ and c: $\beta\hbar\omega=\pi$; $\triangle$ and d: $\beta\hbar\omega=1.8\pi$; $\bigstar$: $\beta\hbar\omega=3\pi$. For $\beta\hbar\omega=0$ and 0.2π, the simulations used $V^{\ddagger}=5k_BT$; for $\beta\hbar\omega=\pi$, 1.8π, and 3π, $V^{\ddagger}=25k_BT$.

parameter $\beta\hbar\omega$. In this region, correlated hops are not important and the diffusion constant depends strongly on the escape rate. Quantum mechanical particles are more likely to tunnel, increasing the escape rate, and D is larger than for a corresponding classical particle.

Correlated hops become important in the underdamped, low friction regime. The increase in the jump length due to correlated hops more than compensates for the reduction in the escape rate, resulting in an increase in the diffusion constant. As seen in the previous section, correlated hops are much more likely and also longer for classical particles than for quantum particles. The classical diffusion constant consequently increases more quickly than the diffusion constant for a quantum particle.

A theoretical analysis predicts that the diffusion constant above the crossover temperature scales as $\delta^{-1+\beta\hbar\omega/2\pi}$ in the weak damping regime.[25] Simulations indicate that this expression is valid for $\delta\lesssim 1$. Finally, these simulation results reinforce the theoretical prediction of an inverse isotope effect: the classical diffusion constant is larger than the quantum diffusion constant when friction is small.

We note that the agreement between theory and simulation for D is better than that for κ for the strongly quantum frequency $\beta\hbar\omega=1.8\pi$. The reason for the agreement here stems from a cancellation of errors in the theory. The value of δ used in the theory is larger than the effective δ in the simulation. In the low friction, small δ regime, this results in a larger escape rate in the theory than the simulation, but also a smaller probability of a correlated hop. The errors are in opposite directions, giving a small net error in the predicted diffusion constant.

The theoretical results for D are only valid above the crossover temperature, $\beta\hbar\omega\leqslant 2\pi$. Our simulation results slightly below crossover, $\beta\hbar\omega=3\pi$, indicate that the diffusion constant is independent of friction in the low friction regime. This is because tunneling from deep in the well is the dominant escape mechanism for diffusing particles. It is evident that for a fixed value of δ and a large enough value of $\beta\hbar\omega$, quantum tunneling can overcome the effects of low friction, making the quantum diffusion constant larger than the classical diffusion constant. One also expects that for an even smaller value of δ, the classical diffusion constant will once again be larger than the quantum diffusion constant.

G. $\langle(l/l_0)^2\rangle$

Results for the mean square number of lattice spacings per jump, $\langle(l/l_0)^2\rangle$, are shown in Fig. 13. This number is obtained from the results for D and κ from reactive flux simulations as $\tilde{D}/\kappa$. The corresponding theoretical quantity is $D/(D_{sd}\Upsilon)$. At moderate to large damping, $\langle(l/l_0)^2\rangle=1$ and each escaping particle only jumps one lattice spacing. For smaller values of the friction, longer jumps become important. We see again that as $\beta\hbar\omega$ increases, the escape is due more and more to tunneling, and the jump length decreases.

Nonlinear, finite barrier height effects are evident in the simulation results for the frequency $\beta\hbar\omega=1.8\pi$. The simulations show a larger mean square length per jump than predicted by theory. The theoretical estimate is based on the value of δ for an escaping particle at the barrier top energy. Tunneling particles travel below the barrier top energy, have a smaller action per traversal of a well than particles near the barrier energy, and therefore have a smaller effective energy loss than particles escaping over the barrier. Since the jump length increases as δ decreases, the actual jump length is slightly larger than predicted by theory.

The mean square jump length increases as δ^{-2} for classical escape, and the theoretical prediction that $\langle(l/l_0)^2\rangle\sim\delta^{-2+\beta\hbar\omega/\pi}$ is borne out by the simulation results. The theoretical scaling law is valid for moderate to weak friction, $\delta\lesssim 1$. At crossover, $\beta\hbar\omega=2\pi$, the theory predicts no dependence of the jump length on friction; for larger frequencies the theory does not converge. The simulation results we present for $\beta\hbar\omega=3\pi$ indicate that the mean

square jump length remains independent of the frictional damping below the crossover temperature, $\beta\hbar\omega > 2\pi$, with $\langle l^2\rangle \approx l_0^2$.

VI. DISCUSSION

We have investigated surface diffusion with a one-dimensional model which allows for the quantum mechanical tunneling and reflection of the diffusing particle. At each turning point or barrier crossing, a semiclassical transmission probability determines whether the particle is transmitted or reflected. We have used a stochastic Langevin equation to model the fluctuations and dissipation of the energy of the diffusing particle.

We have developed a reactive flux method to efficiently investigate surface diffusion when the barrier between wells is large. The standard reactive flux method for classical systems is no longer valid when particles can tunnel. Classically, each reactive flux trajectory starts at the top of the barrier with energy greater than the barrier energy. Semiclassical tunneling serves to broaden the initial distribution of the reactive flux trajectories. The modification to the classical reactive flux algorithm can be described as replacing the classical transmission probability, 1 if the energy is above the barrier and 0 otherwise, with the semiclassical transmission probability $T(E)$.

Reactive flux methods require that trajectories be continued up to a plateau time, the time for a reactive particle starting near a barrier to be thermalized in a well. When the frictional damping of the particle is small, the regime emphasized here, the plateau time can be quite long. We have vastly increased the efficiency of our sampling of trajectories by developing a new multiple time step method. Each time step in this method corresponds to the time for a particle to traverse a well at constant energy. Coupling to the frictional bath is incorporated as a stochastic perturbation to the conservative reference trajectory. This method can increase computational speed by a factor of 100.

Our simulation results are compared to theoretical predictions for the escape rate, escape energy, and diffusion constant. We find that the theoretical predictions are almost always in perfect agreement with the simulation results. The simulation and theory disagree only near the crossover between activated tunneling and deep tunneling, when the reduced barrier frequency $\beta\hbar\omega$ approaches 2π. The simulations demonstrate that near crossover, the finite height and nonlinearity of the barrier between wells become important. The theory presented here is based on a parabolic extrapolation from the top of the barrier, and predicts an escape rate that is too large. Theory also predicts a jump length that is too large, however, and the cancellation of errors results in a diffusion constant which is quite accurate.

The simulations also provide results where the theory no longer converges, i.e. below the crossover temperature. We find that the limiting behavior of the diffusion constant predicted by theory at crossover continues below crossover as well. It is possible to develop theoretical approaches which converge at and below the crossover temperature; these methods will be described elsewhere.

The simulation results support the prediction that reducing friction increases the diffusion constant. Furthermore, for sufficiently small friction, the classical diffusion constant is larger than the quantum. Although quantum particles have a larger escape rate due to tunneling through the barrier between wells, above-barrier reflection reduces the length of correlated hops for quantum particles relative to classical particles. Therefore, while this reduction to the diffusion constant due to above-barrier reflection is reminiscent of the possibility of quantum reflection reducing the escape rate from a well relative to a classical prediction,[51] it occurs through a different mechanism.

The model described here is one-dimensional. This is a reasonable first approximation since many studies indicate that adsorbates can have a preferential axis for diffusion. Two recent examples are the direct STM observations of Pb diffusion on Ge(111)[16] and simulation studies of H atoms on the Si(100)-2×1 surface.[52] Furthermore, when long hops are important, simulations indicate that the jumps are along a persistent direction.[17,53–55] Simulations also indicate that an effective one-dimensional reaction path potential surface can be a good approximation for the motion of H on a rigid Cu surface.[54] Fully three-dimensional treatments of adsorbate motion have shown a substantial fraction of long hops, $P_1 \approx 0.45$ for H on Ni(100),[56] and that correlated hops can enhance the diffusion constant by a factor of 2 to 3.[57] We are extending our one-dimensional treatment to diffusion on a two-dimensional surface to determine to what extent coupling between Cartesian dimensions can quench long jumps.

The bath in the simulations is strictly classical. We have checked that the theoretical predictions are not sensitive to the treatment of the bath; a classical bath and a quantum bath give the same results for the diffusion constant, the escape rate, etc. This is because the most important quantity characterizing the bath is δ, the average energy loss of the particle to the bath per period, and δ is the same for a classical or quantum bath. Thus, for the Ohmic friction we consider, a quantum treatment of the bath modes would not be likely to produce a substantial change in the simulation results. Replacing the classical bath with a quantum bath would require that the Langevin equation be replaced by a generalized Langevin equation, and that the stochastic random force be replaced by a stochastic operator satisfying a nonclassical fluctuation–dissipation theorem.[58–61] It would be a challenge to simulate this type of quantum generalized Langevin equation. It would not be too difficult, however, to include the quantum aspects of the bath in an energy space simulation by using a quantum $P(E|E')$ kernel rather than the kernel for a classical bath.

The dynamical simulations we have described do not include quantization of energy levels of the particle. The number of bound states per well is given approximately by $[\text{action}/2\pi\hbar]$, or $4\beta V^{\ddagger}/\pi\beta\hbar\omega$ for the cosine potential. For the larger frequencies we consider here, $\beta\hbar\omega \gtrsim \pi$, the number of energy levels is not large, indicating that quantization of energy levels might be important. The dynamical simulations are only used to obtain correction factors to transition state rates, however, and the transition state rates do include quantization of system levels in the well and bath levels both

in the well and at the barrier through the factor Ξ. This ratio of quantum to classical partition functions includes the reduction in the activation energy due to the zero-point energy of the escaping particle, which should be the dominant effect arising from quantization of energy levels. In the deep tunneling regime below crossover, it is likely that an exact description of the escape rate requires quantization of the adsorbate motion in energy levels in each well. A tight-binding model involving coupled sites might be a more appropriate starting point than the semiclassical dynamics described here. The approximation here of incoherent hops between sites might break down, and it might be necessary to describe the diffusion in terms of coherent motion in bandlike states.[62,63]

A number of other approaches have been used to investigate diffusion on a multidimensional surface. Semiclassical transition state theory calculations estimate a quantum mechanical diffusion rate by performing a thermal average of the multidimensional tunneling probability $T(E)$.[64] Centroid methods can also be used to estimate a quantum mechanical transition state theory rate constant.[65–68] Although both of these approaches can provide accurate values for rate constants,[69] neither includes a direct estimate of the dynamical effects which lead to long correlated hops. Dynamical effects have been estimated by running classical trajectories on effective potential energy surfaces and with initial conditions chosen from semiclassical distributions.[70–72] These methods do not accurately describe quantum tunneling or reflection beyond the initial barrier crossing. A fully quantum mechanical description of a diffusing particle is possible using basis set methods to evaluate a flux–flux autocorrelation function,[54,56,73] but so far has been limited to a rigid substrate. Real-time path integral methods might allow for a fully quantum mechanical treatment of a diffusing particle and the substrate, with the substrate modes treated as an effective bath of harmonic oscillators.[74–76] It might be difficult, however, to extend real-time path integration to times sufficiently long to encompass a correlated hop.

As a practical manner, escape rates and diffusion constants can be quite sensitive to quantitative details of the adsorbate/surface interactions. These include the relaxation of surface atoms around an impurity, the coupling of the adsorbate to phonon modes, and the effects of nonadiabatic excitations of electron-hole pairs in the solid.[55,56,68]

ACKNOWLEDGMENT

This work has been supported by a grant from the Minerva foundation.

APPENDIX A: THE QUANTUM KERNEL

The quantum extension of PGH theory[33] relies heavily on the normal mode transformation[31] around the barrier top of the Hamiltonian equivalent of the GLE,

$$H=\frac{p_q^2}{2}+w(q)+\sum_j \frac{1}{2}\left[p_{x_j}^2+\left(\omega_j x_j-\frac{c_j q}{\omega_j}\right)^2\right] \tag{A1}$$

from the mass-weighted original system and bath coordinates $(q,x_j;j=1,\ldots)$ to the normal modes $(\rho,y_j;j=1,\ldots)$. The matrix element (u_{00}) projecting the mass-weighted system coordinate onto the unstable normal mode ρ associated with the barrier frequency $\lambda^{\ddagger}$ [cf. Eq. (2.4)], is given in terms of the Laplace transform of the time dependent friction as

$$u_{00}^2=\left[1+\frac{1}{2}\left(\frac{\hat{\gamma}(\lambda^{\ddagger})}{\lambda^{\ddagger}}+\frac{\partial\hat{\gamma}(s)}{\partial s}\bigg|_{s=\lambda^{\ddagger}}\right)\right]^{-1}. \tag{A2}$$

The spectral density of the normal modes, $I(\lambda)$,[28] may be expressed similarly:

$$I(\lambda)=\frac{1}{\lambda}\,\mathrm{Re}[\hat{K}(i\lambda)], \tag{A3}$$

where $[\hat{K}(i\lambda)]$ is the transform of the friction function of the normal modes and is related to the time dependent friction:

$$\hat{K}(s)=\frac{1}{u_{00}^2}\frac{s}{s^2+s\,\hat{\gamma}(s)-\omega^2}-\frac{s}{s^2-\lambda^{\ddagger 2}}. \tag{A4}$$

To determine the quantum kernel it is necessary to solve the equation of motion for the trajectory which at time $-\infty$ is initiated at barrier 1 and as time goes to ∞ it goes asymptotically to the adjacent barrier. This trajectory obeys the zero order equation of motion for the unstable normal mode [cf. Eq. (3.15) of Ref. 33 or Section 2 of Ref. 28]:

$$\ddot{\rho}-\lambda^{\ddagger 2}\rho=-u_{00}\frac{dw_1(q)}{dq}\bigg|_{q=u_{00}\rho}\equiv F(t), \tag{A5}$$

where $w_1(q)$ is the nonlinear part of the potential,

$$w_1(q)\equiv w(q)-[w(q^{\ddagger})-\tfrac{1}{2}\,\omega^2(q-q^{\ddagger})^2], \tag{A6}$$

and $q^{\ddagger}$ denotes the location of the barrier. The power spectrum of the force $F(t)$ along the critical trajectory is defined as

$$\tilde{F}(\lambda)\equiv\left|\int_{-\infty}^{\infty}dt e^{i\lambda t}F(t)\right|^2. \tag{A7}$$

As shown in Ref. 28, the exponent of the quantum kernel has the general form:

$$r(t)=\frac{1}{2\pi\hbar}\int_{-\infty}^{\infty}d\lambda\,\frac{I(\lambda)\tilde{F}(\lambda)[\cosh(\frac{1}{2}\hbar\beta\lambda)-\cos(t\hbar\beta\lambda)}{\sinh(\frac{1}{2}\hbar\beta\lambda)}. \tag{A8}$$

The numerical work in this paper is based on Ohmic friction [Eq. (2.33)]. Using the notation

$$\alpha\equiv\frac{\gamma}{2\omega} \tag{A9}$$

one has the well known Kramers result for the reactive frequency [Eq. (2.4)]:

$$\frac{\lambda^{\ddagger}}{\omega}=(1+\alpha^2)^{1/2}-\alpha. \tag{A10}$$

We denote the second solution of the Kramers equation as:

$$\frac{\lambda_+}{\omega}=(1+\alpha^2)^{1/2}+\alpha. \tag{A11}$$

The spectral density of the normal modes is now easily obtained:

$$I(\lambda)=\frac{\lambda}{2\lambda^{\ddagger}}\left(\frac{1}{\lambda^2+\lambda^{\ddagger 2}}-\frac{1}{\lambda^2+\lambda_+^2}\right). \tag{A12}$$

To proceed further one must use the specific form of the potential, which in our case is the cosine potential of Eq. (2.35). The explicit time dependence for the trajectory that starts asymptotically at $t=-\infty$ at the first barrier and ends at $t=\infty$ at the second barrier is needed for the effective force (A5). To obtain this trajectory we will use the weak damping limit of the equation of motion, which means effectively setting $\lambda^{\ddagger}=\omega^{\ddagger}, u_{00}=1, \rho=q$ in Eq. (A5). This trajectory is at the barrier top energy $E=0$ so that an analytic solution is readily obtained by integrating $dt/(dq)=[-2w(q)]^{-1/2}$. The result is

$$\sin\left[\frac{\omega^{\ddagger}}{(2V^{\ddagger})^{1/2}}q\right]=\tanh(\omega^{\ddagger}t). \tag{A13}$$

In this weak damping limit, the force $F(t)$ is also determined by the unperturbed system trajectory:

$$F(t)=\frac{dw}{dq}+\omega^{\ddagger 2}(q-q^{\ddagger}), \tag{A14}$$

where the time dependence of q is given in Eq. (A13). Obtaining $\tilde{F}(\lambda)$ [cf. Eq. (A7)] is not too difficult. The integrals are tabular integrals, the only trick is that the integration of the linear term in q should be done by parts, the surface term vanishes, the second term involves $\dot{q}$ which is easily expressed through energy conservation. The result is rather simple:

$$\tilde{F}(\lambda)=\frac{2\pi^2 V^{\ddagger}}{\omega^{\ddagger 2}}\frac{(\omega^{\ddagger 2}+\lambda^2)^2}{\lambda^2}\frac{1}{\cosh^2\left(\frac{\pi\lambda}{2\omega^{\ddagger}}\right)}. \tag{A15}$$

Finally, one does not need the exact $I(\lambda)$ for the Ohmic friction as in Eq. (A12) but only the leading order term in the damping γ. This is easily seen to be

$$I(\lambda)\simeq\frac{\gamma\lambda}{(\lambda^2+\omega^{\ddagger 2})^2}. \tag{A16}$$

At this point we obtain the following explicit expression for the exponential factor $r(t)$ that appears in the quantum kernel given in Eq. (2.39). Finally, we note that the energy loss for the cosine potential is just:

$$\delta=\gamma\int_{-l_0/2}^{l_0/2}dq[-2w(q)]^{1/2}=8\beta V^{\ddagger}\alpha. \tag{A17}$$

Although we have used only the weak damping limit of the PGH formalism, for Ohmic friction, previous experience has shown that differences are small. In the underdamped limit, the results used here are anyway exact: as the damping increases both the PGH formalism as well as its 'weak damping' limit as used here lead to large energy losses and so almost identical results. This may be seen explicitly for example in Ref. 77.

APPENDIX B: PERTURBATION THEORY FOR ENERGY FLUCTUATIONS

When frictional damping is weak, the fluctuations in the energy of a particle can be described by a perturbation theory. The rate of change of the energy of a particle obeying Eq. (3.1) is

$$\frac{dE}{dt}=\frac{dV}{dq}\frac{dq}{dt}+\frac{m}{2}\frac{d(\dot{q}^2)}{dt}=m\dot{q}[(1/m)dV/dq+\ddot{q}]$$
$$=m\dot{q}[-\gamma\dot{q}+R(t)]. \tag{B1}$$

To obtain the average rate of change, the random force $R(t)$ must be averaged,

$$\langle dE/dt\rangle_R=-m\gamma\langle\dot{q}^2\rangle_R+m\langle\dot{q}(t)R(t)\rangle_R. \tag{B2}$$

The subscript R indicates an average over the history of the random force $R(t)$. Now we assume that $q(t)$ can be expressed as a power series in $\sqrt{\gamma}$ (note that $R(t)$ is $\mathcal{O}(\sqrt{\gamma})$):

$$q(t)=q_0(t)+\sqrt{\gamma}q_1(t)+\mathcal{O}(\gamma). \tag{B3}$$

At time $t=0$, $q_1(t)=\dot{q}_1(t)=\cdots=0$. Writing $F(q)=-m^{-1}dV/dq$, $F_0(t)=F[q_0(t)]$, $F_1(t)=dF_0(t)/dq_0(t)$, and collecting terms of $\mathcal{O}(1)$ and of $\mathcal{O}(\sqrt{\gamma})$ in the Langevin equation, one finds the equations of motion

$$\ddot{q}_0(t)=F_0(t); \tag{B4}$$

$$\sqrt{\gamma}\ddot{q}_1(t)=\sqrt{\gamma}q_1(t)F_1(t)+R(t). \tag{B5}$$

Clearly q_0 satisfies the conservative equation of motion with $\gamma=0$. Thus to lowest order in γ, the first term in Eq. (B2) is $-\gamma m\dot{q}_0(t)^2$. To lowest order in γ the second term is

$$m\langle\dot{q}_0(t)R(t)\rangle_R+m\langle\sqrt{\gamma}\dot{q}_1(t)R(t)\rangle_R$$
$$=m\left\langle\int_0^t dt'\sqrt{\gamma}\ddot{q}_1(t')R(t)\right\rangle_R, \tag{B6}$$

since $q_0(t)$ is independent of $R(t)$, and R has zero mean. The remaining term can be expanded by noting that

$$\sqrt{\gamma}\ddot{q}_1(t)=R(t)+\sqrt{\gamma}q_1(t)F_1(t)$$
$$=R(t)+F_1(t)\int_0^t dt'\sqrt{\gamma}\dot{q}_1(t')$$
$$=R(t)+F_1(t)\int_0^t dt'\int_0^{t'}dt''R(t'')+\cdots \tag{B7}$$

Finally, performing the average over R,

$$m\left\langle \int_0^t dt'\sqrt{\gamma}\ddot{q}_1(t')R(t)\right\rangle_R = m\left\langle \int_0^t dt' R(t')R(t)\right\rangle_R + m\left\langle \int_0^t dt' F_1(t')\int_0^{t'} dt''\int_0^{t''} dt'''R(t''')R(t)\right\rangle_R + \cdots$$

$$= \gamma/\beta + m\int_0^t dt' F_1(t')\int_0^{t'} dt''\int_0^{t''} dt'''(2\gamma/\beta m)\,\delta(t'''-t) + \cdots$$

$$= \gamma/\beta + 2\gamma/\beta\int_0^t dt'''\int_{t'''}^t dt''\int_{t''}^t dt' F_1(t')\,\delta(t'''-t) + \cdots = \gamma/\beta. \tag{B8}$$

The average energy change Δ is obtained by integration:

$$\Delta = \int_0^t dt'\langle dE/dt'\rangle_R$$

$$= -\gamma\int_0^t dt' m\dot{q}_0(t')\dot{q}_0(t') + \int_0^t dt'\,\gamma/\beta$$

$$= -\gamma\int_{q_0(0)}^{q_0(t)} dq\,p(q) + \gamma t/\beta. \tag{B9}$$

The momentum $p(q)$ is $\sqrt{2[E-V(q)]/m}$.

In the weak damping limit, the first term in Eq. (B9) is exactly the average energy loss δ which appears in Eq. (2.9), derived from considerations of the energy loss of the unstable normal mode. The first term in Δ must therefore be the asymptotic limit for the average change in energy for a trajectory traveling at the barrier top energy as the barrier height increases.

The second term in the perturbation theory will only be valid for short times, $\gamma t \ll 1$, and will induce finite barrier corrections to the standard estimates for the escape rate. This term describes the flow of energy back into the system from the bath. For a physical picture of this term, imagine that V is a harmonic potential $(1/2)m\omega^2 q^2$, that $q_0(0)$ and $q_0(t)$ are the left and right turning points for energy E, and that $t=\pi/\omega$. Defining $J(E)$ as the action for the trajectory which goes from the left turning point to the right turning point in time π/ω,

$$\Delta(E) = -\gamma J(E) + \gamma J(k_B T), \tag{B10}$$

since J for a harmonic oscillator is simply tE. When $E<k_BT$ the harmonic oscillator gains energy on average, and when $E>k_BT$ the oscillator loses energy on average.

As seen explicitly in the example of the harmonic oscillator, the function of the second term in Eq. (B9) is to maintain the proper distribution of energies deep in the well. Furthermore, deep in the well, the period is finite, motion is quasi-harmonic, and $\gamma t/\beta \approx \gamma J(k_BT)$, where the action $J(k_BT)$ is for a period of motion in the full nonlinear potential for a particle energy of $1\ k_BT$. Therefore we adopt Eq. (B10) as our expression for Δ, with the action evaluated at the indicated energies for undamped motion in the potential $V(q)$.

Higher moments of the change in energy for a trajectory can also be calculated from the Langevin equation. First, to lowest order in γ, $dE/dt - \langle dE/dt\rangle_R = m\dot{q}_0(t)R(t)$. The second moment σ^2 of the distribution of energy $E(t)$ given energy E at time 0 is then

$$\sigma^2 = \langle [E(t)-(E+\Delta)]^2\rangle_R$$

$$= \int_0^t dt'\int_0^t dt'' m\dot{q}_0(t')m\dot{q}_0(t'')\langle R(t')R(t'')\rangle_R$$

$$= 2\gamma k_B T\int_0^t m\dot{q}_0(t)\dot{q}_0(t)$$

$$= 2\gamma k_B T\int_{q_0(0)}^{q_0(t)} dq\,p(q). \tag{B11}$$

Furthermore, since R is a Gaussian random variable, $dE/dt - \langle dE/dt\rangle_R$ is a Gaussian random variable, and the fluctuations of $E(t)$ about $E+\Delta$ must also be Gaussian. Therefore, in the limit of weak damping, the probability distribution of $E(t)$ is a Gaussian uniquely determined by the first moment Δ and second moment σ^2.

This Gaussian form of the transition kernel P does not obey detailed balance,

$$P(E|E')\exp[-\beta E'] \neq P(E'|E)\exp[-\beta E]. \tag{B12}$$

The kernel is not microscopically reversible because the parameters Δ and σ^2 are not symmetric in their dependence on E and E'. The error made at each step can be estimated as

$$\text{error} = \frac{P(E|E')\exp(-\beta E')}{P(E'|E)\exp(-\beta E)} - 1, \tag{B13}$$

where E is the energy at the start of the step and E' is the new energy chosen from the distribution $P(E'|E)$. One can show that $\langle \text{error}\rangle \propto \langle E'-E\rangle \propto \delta$, where δ is the energy loss at the barrier top energy. The cumulative systematic error after N steps scales as $N\delta$. The number of steps N required to follow an activated trajectory until it is trapped in a well scales like $1/\delta$. Thus, to lowest order in δ, the cumulative error over the length of a trajectory from activation until thermalization should be independent of δ: even though more steps are needed for a smaller δ, the error per step is smaller, and the δ-dependence cancels out.

We have tested the importance of deviations from detailed balance by performing simulations using both Langevin dynamics and energy space dynamics at an intermediate value of the friction γ corresponding to the reduced energy loss $\delta=1$. We found agreement in the results of these two simulation methods, indicating that the energy space dynamics simulations should also be accurate for smaller values of γ.

[1] J. C. Tully, Annu. Rev. Phys. Chem. **31**, 319 (1980).
[2] H. Risken, *The Fokker–Planck Equation* (Springer, Berlin, 1989).
[3] T. Yamamoto, J. Chem. Phys. **33**, 281 (1960).
[4] J. C. Keck, Adv. Chem. Phys. **13**, 85 (1967).
[5] J. B. Andersen, J. Chem. Phys. **58**, 4684 (1973).
[6] C. H. Bennett, in *Algorithms for Chemical Computation*, edited by R. E. Christofferson (American Chemical Society, Washington, DC, 1977).
[7] D. Chandler, J. Chem. Phys. **68**, 2959 (1978).
[8] J. A. Montgomery, Jr., D. Chandler, and B. J. Berne, J. Chem. Phys. **70**, 4056 (1979).
[9] A. F. Voter and J. D. Doll, J. Chem. Phys. **82**, 80 (1985).
[10] A. F. Voter, J. D. Doll, and J.M. Cohen, J. Chem. Phys. **90**, 2045 (1989).
[11] P. Hänggi, P. Talkner, and M. Borkovec, Rev. Mod. Phys. **62**, 251 (1990).
[12] B. J. Berne, in *Activated Barrier Crossing*, edited by G. R. Fleming and P. Hänggi (World Scientific, New York, 1993).
[13] M. E. Tuckerman and B. J. Berne, J. Chem. Phys. **95**, 4389 (1991).
[14] S. C. Tucker, M. E. Tuckerman, B. J. Berne, and E. Pollak, J. Chem. Phys. **95**, 5809 (1991).
[15] M. Tuckerman, B. J. Berne, and G. J. Martyna, J. Chem. Phys. **97**, 1990 (1992).
[16] E. Ganz, S. K. Theiss, I.-S. Hwang, and J. Golovchenko, Phys. Rev. Lett. **68**, 1567 (1992).
[17] K. D. Dobbs and D. J. Doren, J. Chem. Phys. **97**, 3722 (1992).
[18] R. Ferrando, R. Spadacini, and G. E. Tommei, Phys. Rev. A **46**, R699 (1992).
[19] R. Ferrando, R. Spadacini, and G. E. Tommei, Surf. Sci. **265**, 273 (1992).
[20] G. J. Moro and A. Polimeno, Chem. Phys. Lett. **189**, 133 (1992).
[21] M. Büttiker, E. P. Harris, and R. Landauer, Phys. Rev. B **28**, 1268 (1983).
[22] E. Pollak, J. S. Bader, B. J. Berne, and P. Talkner, Phys. Rev. Lett. **70**, 3299 (1993).
[23] V. I. Mel'nikov, Phys. Rep. **209**, 1 (1991).
[24] V. I. Mel'nikov and A. Sütö, Phys. Rev. B **34**, 1514 (1986).
[25] Y. Georgievskii and E. Pollak, Phys. Rev. E **49**, 5098 (1994).
[26] V. I. Goldanskii, Dokl. Akad. Nauk SSSR **124**, 1261 (1959).
[27] V. I. Goldanskii, Dokl. Akad. Nauk SSSR **127**, 1037 (1959).
[28] I. Rips and E. Pollak, Phys. Rev. A **41**, 5366 (1990).
[29] R. F. Grote and J. T. Hynes, J. Chem. Phys. **73**, 2715 (1980).
[30] P. Hänggi and F. Mojtabai, Phys. Rev. A **26**, 1168 (1982).
[31] E. Pollak, J. Chem. Phys. **85**, 865 (1986).
[32] P. G. Wolynes, Phys. Rev. Lett. **47**, 968 (1981).
[33] E. Pollak, H. Grabert, and P. Hänggi, J. Chem. Phys. **91**, 4073 (1989).
[34] V. I. Mel'nikov and S. V. Meshkov, J. Chem. Phys. **85**, 1018 (1986).
[35] H. Dekker, Phys. Rev. A **38**, 6351 (1988).
[36] M. P. Allen and D. J. Tildesley, *Computer Simulation of Liquids* (Oxford University Press, New York, 1987).
[37] S. Chandrasekhar, Rev. Mod. Phys. **15**, 1 (1943); reprinted in *Selected Papers on Noise and Stochastic Processes*, edited by N. Wax (Dover, New York, 1954).
[38] Some simulations were performed by setting E' to E_0 when sampling produced an energy smaller than E_0. This small difference in the sampling scheme did not influence any results we report.
[39] M. E. Tuckerman and B. J. Berne, J. Chem. Phys. **95**, 8362 (1991).
[40] M. Tuckerman and B. J. Berne, J. Chem. Phys. **98**, 7301 (1993).
[41] E. C. Kemble, *The Fundamental Principles of Quantum Mechanics* (McGraw-Hill, New York, 1937).
[42] L. D. Landau and E. M. Lifshitz, *Quantum Mechanics (Non-relativistic Theory)*, 3rd ed. (Pergamon, New York, 1977).
[43] R. A. Harris and L. Stodolsky, J. Chem. Phys. **74**, 2145 (1981).
[44] A. O. Caldeira and A. J. Leggett, Phys. Rev. Lett. **46**, 211 (1981).
[45] A. O. Caldeira and A. J. Leggett, Ann. Phys. (N.Y.) **149**, 374 (1983), **153**, 445 (Errata).
[46] V. I. Mel'nikov and S. V. Meshkov, JETP Lett. **38**, 130 (1983).
[47] P. Hänggi, H. Grabert, G. L. Ingold, and U. Weiss, Phys. Rev. Lett. **55**, 761 (1985).
[48] J. T. Hynes, J. Phys. Chem. **90**, 3701 (1986).
[49] E. Pollak, Phys. Rev. A **33**, 4244 (1986).
[50] J. S. Bader and B. J. Berne, J. Chem. Phys. (submitted).
[51] U. Griff, H. Grabert, P. Hänggi, and P. S. Riseborough, Phys. Rev. B **40**, 7295 (1989).
[52] C. J. Wu and E. A. Carter, Phys. Rev. B **46**, 4651 (1992).
[53] M. J. Gillan, J. Phys. C **19**, 6169 (1986).
[54] K. Haug, G. Wahnström, and H. Metiu, J. Chem. Phys. **92**, 2083 (1990).
[55] Y. Li and G. Wahnström, Phys. Rev. B **46**, 14528 (1992).
[56] K. Haug and H. Metiu, J. Chem. Phys. **94**, 3251 (1991).
[57] Z. Zhang, K. Haug, and H. Metiu, J. Chem. Phys. **93**, 3614 (1990).
[58] P. S. Riseborough, P. Hänggi, and U. Weiss, Phys. Rev. A **31**, 471 (1985).
[59] E. Cortés, B. J. West, and K. Lindenberg, J. Chem. Phys. **82**, 2708 (1985).
[60] G. W. Ford and M. Kac, J. Stat. Phys. **46**, 803 (1987).
[61] G. W. Ford, J. T. Lewis, and R. F. O'Connell, Phys. Rev. A **37**, 4419 (1988).
[62] P. D. Reilly, K. B. Whaley, and R. A. Harris, J. Chem. Phys. **95**, 8599 (1991).
[63] P. D. Reilly, K. B. Whaley, and R. A. Harris, J. Chem. Phys. **97**, 6975 (1992).
[64] J. G. Lauderdale and D. G. Truhlar, J. Am. Chem. Soc. **107**, 4590 (1985).
[65] M. J. Gillan, J. Phys. C **20**, 3621 (1987).
[66] G. A. Voth, D. Chandler, and W. H. Miller, J. Chem. Phys. **91**, 7749 (1989).
[67] G. A. Voth, D. Chandler, and W. H. Miller, J. Phys. Chem. **93**, 7009 (1989).
[68] Y. C. Sun and G. A. Voth, J. Chem. Phys. **98**, 7451 (1993).
[69] R. P. McRae, G. K. Schenter, B. C. Garrett, G. R. Haynes, G. A. Voth, and G. C. Schatz, J. Chem. Phys. **97**, 7392 (1992).
[70] J. D. Doll, J. Chem. Phys. **81**, 3536 (1984).
[71] G. K. Schenter, M. Messina, and B. C. Garrett, J. Chem. Phys. **99**, 1674 (1993).
[72] D. E. Sagnella, J. S. Cao, and G. A. Voth, Chem. Phys. Lett. **180**, 167 (1994).
[73] W. H. Miller, S. D. Schwartz, and J. W. Tromp, J. Chem. Phys. **79**, 4889 (1983).
[74] R. Egger and C. H. Mak, J. Chem. Phys. **99**, 2541 (1993).
[75] C. H. Mak and J. N. Gehlen, Chem. Phys. Lett. **206**, 130 (1993).
[76] M. Topaler and N. Makri, Chem. Phys. Lett. **210**, 285 (1993).
[77] S. Linkwitz, H. Grabert, E. Turlot, D. Estève, and M. H. Devoret, Phys. Rev. B **45**, R3369 (1992).